Spring 2019

A Framework to Analyze Energy Efficiency of Multi-Band Spectrum Sensing Algorithms

Jay Bhadresh Patel
San Jose State University

A FRAMEWORK TO ANALYZE ENERGY EFFICIENCY OF MULTI-BAND SPECTRUM SENSING ALGORITHMS

A Thesis

Presented to

The Faculty of the Department of Electrical Engineering

San José State University

In Partial Fulfillment

of the Requirements for the Degree

Master of Science

by

Jay B. Patel

May 2019

The Designated Thesis Committee Approves the Thesis Titled

A FRAMEWORK TO ANALYZE ENERGY EFFICIENCY OF MULTI-BAND SPECTRUM SENSING ALGORITHMS

by

Jay B. Patel

APPROVED FOR THE DEPARTMENT OF ELECTRICAL ENGINEERING

SAN JOSÉ STATE UNIVERSITY

May 2019

Birsen Sirkeci, Ph.D.	Department of Electrical Engineering
Robert H. Morelos-Zaragoza, Ph.D.	Department of Electrical Engineering
Sotoudeh Hamedi-Hagh, Ph.D.	Department of Electrical Engineering

ABSTRACT

A FRAMEWORK TO ANALYZE ENERGY EFFICIENCY OF MULTI-BAND SPECTRUM SENSING ALGORITHMS

by Jay B. Patel

Cognitive radio (CR) is a device which can detect wireless communication channels that are not in use and adapt its parameters intelligently. Networks with CRs use the available frequency bands much more efficiently and hence have higher data rates compare to traditional radios. Spectrum sensing is the class of techniques used by CRs to understand its wireless environment. Recent research on evaluating multi-band spectrum sensing algorithms is limited to only algorithm complexity and optimization; therefore, the primary goal of the study is to devise a novel framework that analyzes a multi-band spectrum sensing algorithm in terms of energy consumption and algorithm efficiency. The proposed structure leads to a comparison and evaluation of a large class of multi-band spectrum sensing algorithms. Multi-band spectrum sensing search methods such as linear, random and binary are evaluated for energy loss and detection performance using the proposed framework.

ACKNOWLEDGMENTS

I want to thank my advisor, Dr. Birsen Sirkeci, for her outstanding support, dedication, and patience throughout the research.

I also like to thank Dr. Robert H. Morelos-Zaragoza and Dr. Sotoudeh Hamedi-Hagh for being committee members. I would also thank Cheryl R. Cowan, SJSU Graduate Studies Associate, for her assistance in directing me to correct resources to correctly and efficiently develop my thesis document.

Last, but not least, I would like to thank my mom. Without her support, I would have never been able to complete this thesis or pursue my dreams.

TABLE OF CONTENTS

List of Tables viii

List of Figures x

List of Abbreviations xi

1 Introduction 1
1.1 Motivation 2
1.2 Research Objectives 2
1.3 Thesis Organization 3

2 Background Knowledge 4
2.1 Power Spectral Density 4
2.2 Signal-to-Noise Ratio 5
2.3 Peak-to-Average Power Ratio 6
2.4 Signal-to-Quantization Noise Ratio 7
2.5 Third-Order Input Intercept Point 8

3 Literature Review 10
3.1 Analysis of Receiver Front End 10
3.1.1 Receiver Architectures 10
3.1.1.1 Heterodyne architecture 11
3.1.1.2 Zero-IF architecture 12
3.1.1.3 Other architectures 13
3.1.2 Receiver Front End Components Analysis 13
3.2 One-Band Spectrum Sensing Methods 19
3.2.1 Energy Detector 20
3.2.2 Cyclostationary Detector 21
3.2.3 Matched Filter Detector 22
3.2.4 Other Methods 24
3.3 Multi-Band Spectrum Sensing for Primary Detection 25
3.3.1 Serial Detector 26
3.3.1.1 Adjustable BPF 26
3.3.1.2 Tunable LO 26
3.3.2 Wavelet Detector 26
3.3.3 Joint Detector 27
3.3.4 Filter Bank-Based Detector 28
3.3.5 Other Detectors 29

4 System Model 31

4.1 Receiver's Operation Status 31
4.2 Receiver Front End Energy Model 33

5 A Framework For The Analysis of Multi-Band Spectrum Sensing 37
5.1 Single Empty Band Detection Performance Framework 37
5.2 Multiple Empty Bands Detection Performance Framework 39

6 Multi-Band Spectrum Sensing Algorithms 42
6.1 Linear Search 42
6.2 Random Search Without Replacement 43
6.3 Random Search With Replacement 44
6.4 Binary Search 45

7 Simulations and Results 48
7.1 Simulation Description 48
7.2 Single Empty-Band Detection Simulations 49
7.3 Multiple Empty-Band Detection Simulations 52

8 Conclusions and Future Work 61

Literature Cited 62

Appendix A: Simulation Algorithm 68

LIST OF TABLES

Table 1. Simulation Environment 48

Table 2. Simulation Notation 68

LIST OF FIGURES

Fig. 1. Power spectral density. 5

Fig. 2. Signal-to-noise ratio. 6

Fig. 3. Peak-to-average power ratio. 7

Fig. 4. Intermodulation distortion. 9

Fig. 5. The third-order input intercept point. 9

Fig. 6. Ideal receiver for CRs. 11

Fig. 7. Simple heterodyne receiver architecture design. 12

Fig. 8. Zero-IF receiver architecture design. 12

Fig. 9. Linear model of analog filters. 14

Fig. 10. Role of a mixer at receiver front end. 16

Fig. 11. ADC power versus sampling rate survey. 18

Fig. 12. Energy detector. 20

Fig. 13. Cyclostationary detector. 22

Fig. 14. Matched filter detector. 23

Fig. 15. Multi-band spectrum sensing. 25

Fig. 16. Wavelet detector. 27

Fig. 17. Joint detector. 28

Fig. 18. Filter bank-based detector. 28

Fig. 19. Receiver operation status monitor. 32

Fig. 20. Receiver front end architecture for energy model. 33

Fig. 21. Linear search. 43

Fig. 22. Random search without replacement. 44

Fig. 23. Random search with replacement. 45

Fig. 24. Binary search. 46

Fig. 25. Energy consumption plots for single empty band detection methods with different SNRs. 50

Fig. 26. Energy consumption plot for single empty band detection methods with different $\hat{n}_{max}$. 51

Fig. 27. Energy consumption and true detection performance analysis of the linear search spectrum sensing method using the FROC and SAA-FROC frameworks. 53

Fig. 28. False detection performance analysis of the linear search spectrum sensing method using the FROC framework. 54

Fig. 29. False detection performance analysis of the linear search spectrum sensing method using the SAA-FROC framework. 55

Fig. 30. Energy consumption and detection performance analysis of the linear search spectrum sensing method using the AFROC framework. 56

Fig. 31. Energy consumption and detection performance analysis of the linear search spectrum sensing method using the SAA-AFROC framework. 57

Fig. 32. FROC analysis plot for the linear and binary search methods. 58

Fig. 33. Energy consumption plots for multiple empty band detection methods with respect to the threshold. 59

LIST OF ABBREVIATIONS

CR	Cognitive Radio
IoT	Internet of Things
PU	Primary User
SU	Secondary User
ISM	Industrial, Scientific, and Medical
LNA	Low Noise Amplifier
BPF	Band Pass Filter
PLL	Phase-Locked Loop
LO	Local Oscillator
LPF	Low Pass Filter
VGA	Variable Gain Amplifier
ADC	Analog-to-Digital Converter
PSD	Power Spectral Density
SNR	Signal-to-Noise Ratio
PAPR	Peak-to-Average Power Ratio
ENOB	Effective Number of Bits
FoM	Figure of Merit
FFT	Fast Fourier Transform
ROC	Receiver Operating Characteristics
LROC	Localized Receiver Operating Characteristics
AUC	Area Under the Curve
GLRT	Generalized Likelihood Ratio Test
FROC	Free Response Receiver Operating Characteristics
SAA-FROC	Signal Absent Abscissa Free Response Receiver Operating Characteristics
AFROC	Alternate Free Response Receiver Operating Characteristics
SAA-AFROC	Signal Absent Abscissa Alternate Free Response Receiver Operating Characteristics

1 INTRODUCTION

The internet of things (IoT) is a group of uniquely identifiable devices connected to the internet via pre-defined protocols. Examples of IoT devices include washing machines, smart thermostats, wearable gadgets, and smart televisions. The development and implementation of smart cities, smart cars, smart homes, and smart grids depends on the advancement of IoT devices. Advancement of wireless communication technology has led to an increase in IoT devices [1].

A cognitive radio (CR), which is a smart radio, continuously obtains knowledge of the surrounding spectrum environment to adjust the radio's operational parameters dynamically. Cognitive radios perform efficient data transmission due to their adaptive behavior. One of the primary goals of the CR in IoT devices is to use empty frequency bands belonging to a licensed primary user (PU) when the PU is not transmitting or receiving any data. The utilization of PU frequency bands by CRs allows an unlicensed secondary user (SU) to transfer the data efficiently. The use of CR in the IoT environment is emerging rapidly due to the dynamic spectrum sensing capability. With the current pace of development in the telecommunication industry, CRs will become a necessary part of the IoT devices soon [2].

Spectrum sensing is a crucial process performed by CRs to determine the presence or the absence of PUs in the frequency bands of interest. One-band spectrum sensing and multi-band spectrum sensing are two categories of the spectrum sensing process. The task of the one-band spectrum sensing method is to examine one band for its availability to transfer the data. Coherent detection, energy detection, cyclostationary detection, second-moment detection, and covariance detection are different strategies to perform one-band spectrum sensing [3]–[6]. The task of a multi-band spectrum sensing method is to find multiple bands that are available to transfer the data. The common multi-band

spectrum sensing methods are linear detectors, parallel detectors, and wide-band detectors as the multi-band spectrum sensing methods [3]–[6].

1.1 Motivation

The increase in wireless IoT devices leads to an increase in data traffic in free industrial, scientific and medical (ISM) bands. Since Wi-Fi technology also relies on ISM bands for data transfer, the ISM bands are no longer reliable bands for wireless IoT devices to operate [2]. The implementation of 5th generation (5G) wireless communication technology drives the rapid deployment of IoT devices. 5G technology addresses many issues related to complex IoT requirements and architectures [7]. Also, 5G technology promises to be faster, cheaper, and more secure compared to previous wireless communication technologies like 4th generation (4G) and long-term evolution (LTE). The main challenges of implementing CRs as IoT devices include high energy consumption of the device, inefficient use of spectrum sensing algorithms and unavailability of the constant power supply. A spectrum sensing algorithm may give the best performance in terms of detection of empty bands, but it consumes more energy. Hence, an energy efficient algorithm with high detection performance is vital to implement a CR as an IoT device in a restrictive energy environment.

Lack of research, a bright future, and open challenges of CRs were the driving force of my investigation into the spectrum sensing framework. There was a need for creating a generalized framework that considers not only the detection performance of the spectrum sensing algorithms but also the energy consumption of the CR.

1.2 Research Objectives

The primary goal of the research is to investigate the energy consumption behavior of the receiver front ends used in CRs. Circuit blocks such as a low noise amplifier (LNA), band-pass filters (BPFs), mixers, a phase-locked loop (PLL) or a local oscillator (LO), low-pass filters (LPFs), a variable gain amplifier (VGA) and an analog-to-digital converter

(ADC) are an integral part of the receiver front end. There are three specific objectives of the research. The first specific objective is to analyze the critical system-level factors that dominate the energy dissipation of the receiver front end circuit blocks. The second specific objective includes the formation of a system-level energy consumption model that can determine the amount of energy loss of a multi-band spectrum sensing algorithm. The third specific objective requires the energy loss model to be compatible with the multi-band detection performance framework so that the comparison between energy loss and detection performance can be made.

1.3 Thesis Organization

The organization of this paper is as follows. In Chapter 2 the background knowledge needed to understand the study is presented. In Chapter 3, the past research on the power dissipation of a receiver front end, one-band spectrum sensing methods and multi-band spectrum sensing methods are discussed in detail. Chapter 4 introduces a system model to analyze the energy consumption of the receiver front end. Chapter 5 serves as a framework to analyze multi-band spectrum sensing algorithms. Chapter 6 defines the algorithms used to present the simulation results. The simulation and results of the proposed research are presented in Chapter 7. Chapter 8 concludes the thesis and mentions potential research areas for further improvement of the study.

2 BACKGROUND KNOWLEDGE

The analysis of receiver front end hardware requires the understanding of essential signal processing concepts. This section presents essential background knowledge to interpret the development and investigation of previous work.

2.1 Power Spectral Density

Signals received at the receiver front end are always random due to thermal noise. A power spectral density (PSD) is the parameter used to evaluate the energy distribution of the received signal over frequency.

$$R_{xx}(\tau) = \mathbf{E}[X(t) \cdot X(t+\tau)] \tag{1}$$

where $\mathbf{E}[.]$ represents the expectation operation, and X is a random process.

$$\begin{aligned} S_{xx}(\omega) &= \int_{-\infty}^{\infty} R_{xx} \cdot (\tau) e^{-j\omega\tau} d\tau \\ S_{xx}(\omega)(\mathrm{dB}) &= 10 \cdot \log_{10}(S_{xx}(\omega)) \end{aligned} \tag{2}$$

Autocorrelation is the correlation of the received signal with its delayed copy as shown in (1). For random signals, the PSD is the Fourier transform of the autocorrelation function defined in (2). Fig. 1 shows the PSD in decibels of a noisy 10 kHz sinusoidal signal.

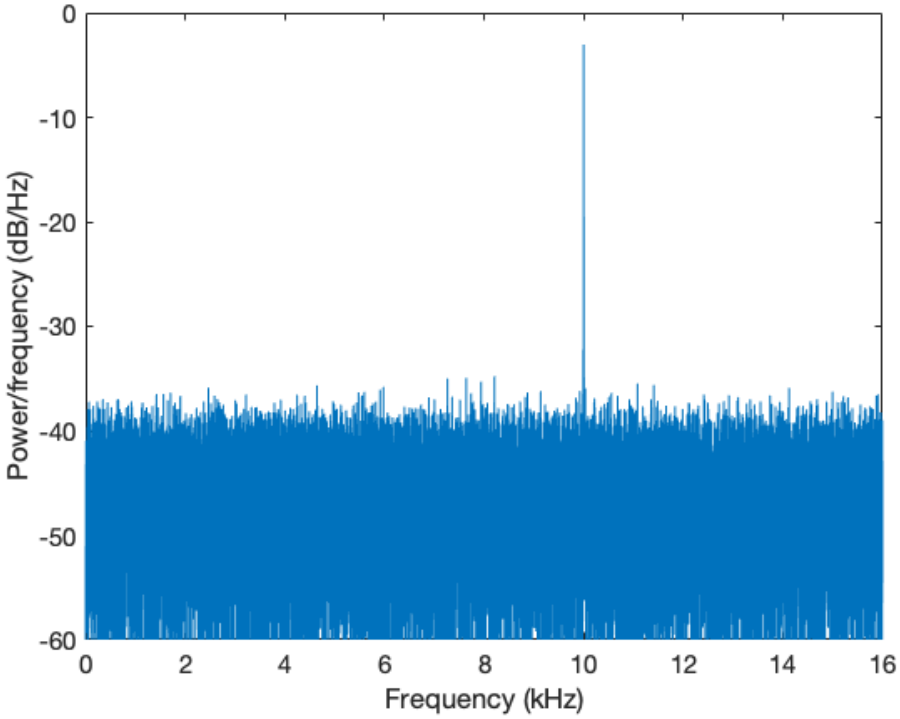

Fig. 1. Power spectral density.

2.2 Signal-to-Noise Ratio

The signal-to-noise ratio (SNR) is a critical parameter in communication systems because the signal received at the receiver front end includes random thermal noise. Therefore, the performance of the receiver depends on the magnitude of the noise power in the received signal.

$$\begin{aligned} \text{SNR} &= \frac{\mathbf{E}[X^2]}{\sigma_N^2} \\ \text{SNR}_{\text{dB}} &= 10 \cdot \log_{10}\left(\frac{\mathbf{E}[X^2]}{\sigma_N^2}\right) \end{aligned} \tag{3}$$

where X is a random signal, and σ_N^2 is the noise variance.

The signal-to-noise ratio is defined as the ratio of the average power of the random signal to the variance of the noise as shown in (3). The SNR is often presented in

decibels. Fig. 2 shows the power of a sinusoidal signal at the frequency of 10 kHz with random noise. The y-axis represents the power of the input signal in the decibel watts, and the x-axis denotes the frequency range in the kilohertz.

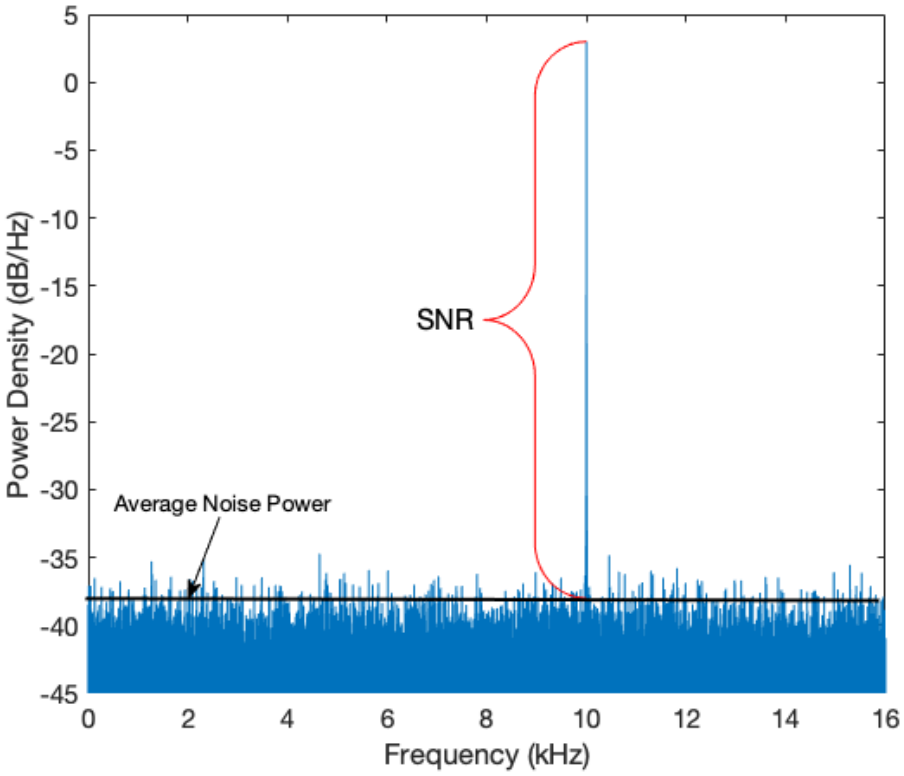

Fig. 2. Signal-to-noise ratio.

2.3 Peak-to-Average Power Ratio

The peak-to-average power ratio (PAPR) gives the information on the distribution of the power of the received signal. The PAPR is defined as the ratio of the peak power of the signal to the RMS value of the signal as

$$\text{PAPR} = \frac{P_{PEAK}}{P_{\text{rms}}}$$
$$\text{PAPR}_{\text{dB}} = 10 \cdot \log_{10}\left(\frac{P_{PEAK}}{P_{\text{RMS}}}\right) \tag{4}$$

where P_{PEAK} is the peak signal power, and P_{RMS} is the root-mean-square (RMS) value of the received signal power.

Generally, the sparse distribution of the signal power is desirable because it relaxes the design complexity of the receiver front end blocks such as mixers and ADCs. A high PAPR degrades the performance of the radio frequency (RF) systems in terms of power dissipation and ADC resolution [8]. Fig. 3 depicts the power of multiple noisy sinusoidal signals with different amplitude and frequency. The y-axis represents the power of the input signals in decibel watts, and the x-axis denotes the frequency range in kilohertz.

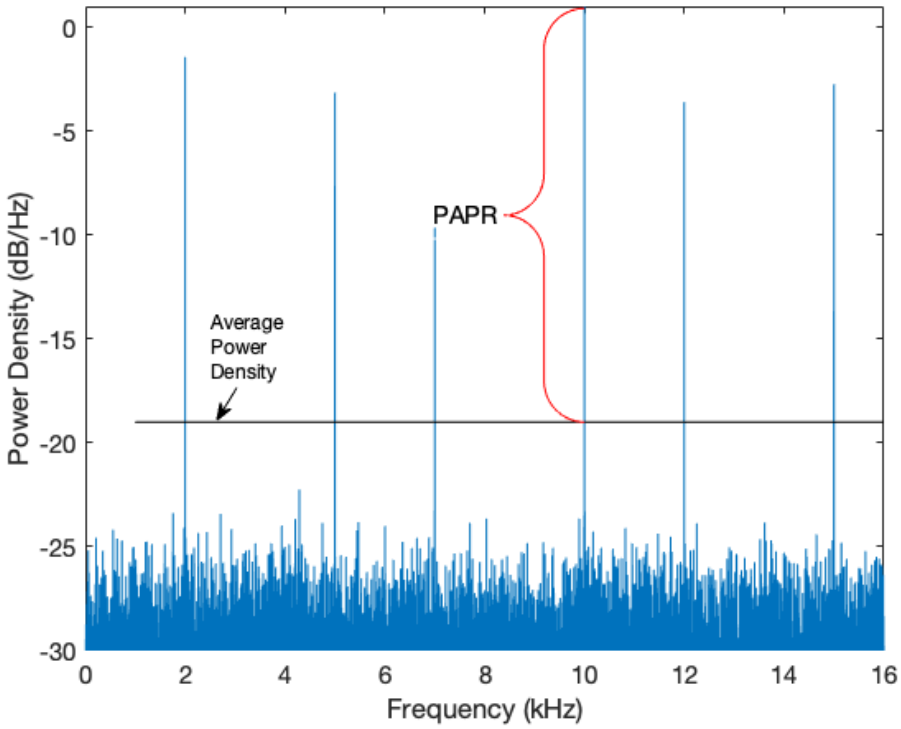

Fig. 3. Peak-to-average power ratio.

2.4 Signal-to-Quantization Noise Ratio

Analog to digital conversion of a received signal by an ADC produces additional quantization noise. Therefore, the signal power is compared with the quantization noise

power to determine the effect of the quantization noise. The signal-to-quantization noise ratio (SQNR) is defined as

$$\text{SQNR} = \frac{P_{Sig}}{P_{\text{QN}}}$$
$$\text{SQNR}_{\text{dB}} = 10 \cdot \log_{10}\left(\frac{P_{Sig}}{P_{\text{QN}}}\right) \tag{5}$$

where P_{Sig} is the signal power,and P_{QN} is the quantization noise.

The high PAPR often degrades the performance of an ADC by reducing the resolution. The effective number of bits (ENOB) is the parameter that is used to measure the resolution of an ADC based on the PAPR and SQNR.

2.5 Third-Order Input Intercept Point

The design of an amplifier for the receiver front end is a challenging task due to non-linearities. The non-linear behavior of the amplifier in the receiver front end introduces the harmonics of the received signal. The third or fourth order does not affect the performance of the amplifier if high harmonics are outside the bandwidth of the amplifier. However, adjacent signals could produce the harmonics that are within the bandwidth of the amplifier. Hence, in addition to primary signals, the harmonics of the received signal also get amplified. The amplified harmonic signals interfere with the signal of interest. As shown in Fig. 4, the green bars are the signals of interest, and the red bar represents the third-order intermodulation products that interfere with concerned signals. The second and third order signal often fall outside the bandwidth of the amplifier.

The third-order input intercept point (IIP3) is a theoretical point. In Fig. 5, the 3-dB intercept point (IP3) is where the fundamental signal power and the third order signal power theoretically intercept. The projection of the IP3 on the input power axis is the IIP3. The IP3 value is the maximum power the amplifier can handle without introducing

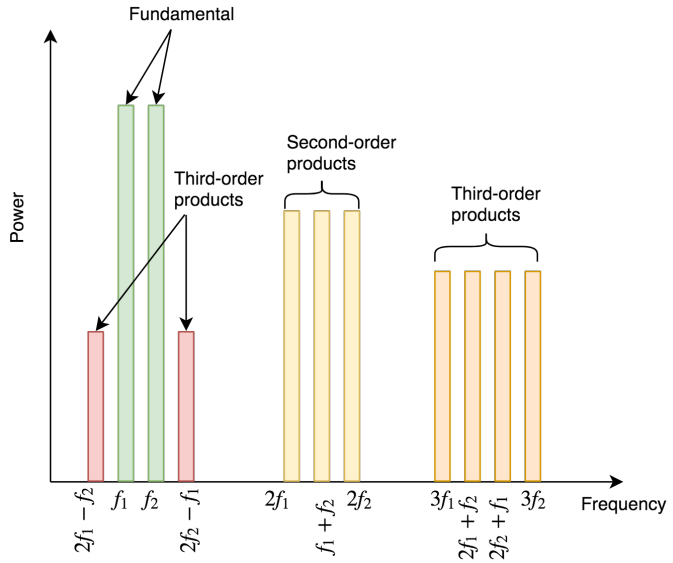

Fig. 4. Intermodulation distortion.

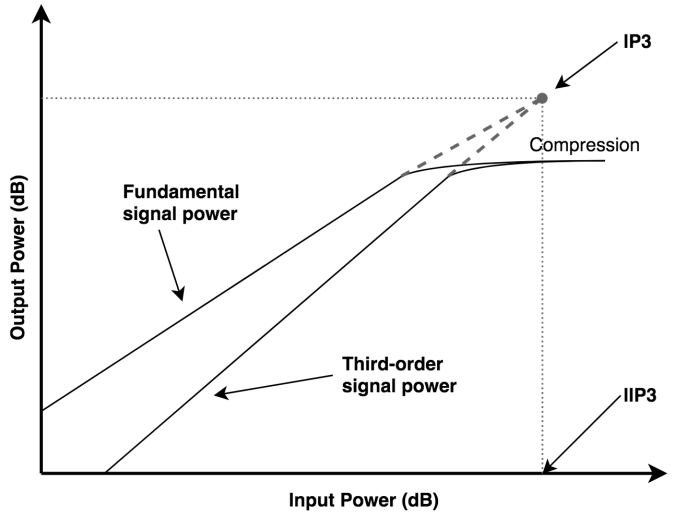

Fig. 5. The third-order input intercept point.

intermodulation effects. Hence, a high IP3 value is usually desirable in the receiver front end amplifier design.

3 LITERATURE REVIEW

Previous work in the field of receiver front end needs to be investigated to understand the energy consumption of critical receiver front end components. The spectrum sensing task can be divided into one-band and multi-band. There are many distinct methods to perform spectrum sensing. In-depth examination of the previously proposed multi-band spectrum sensing methods is key to this research.

3.1 Analysis of Receiver Front End

In digital communication systems, a signal received at the antenna passes through many analog circuit blocks before being processed by a digital processor. The group of RF circuitry that processes the received signal until discretization is called receiver front end. The receiver front end has many types and contains many circuit components. This section presents the previous work done to analyze the power consumption of the receiver front end used in CRs.

3.1.1 Receiver Architectures

As shown in Fig. 6, a typical receiver architecture has a reconfigurable antenna, a high dynamic range LNA and ADCs. The baseband processor does the down conversion and the baseband processing of the received signal. However, the implementation of the reconfigurable antenna and a wideband LNA is challenging and inefficient [9]. Also, the ADC required in the ideal receiver needs high sampling rates. Therefore, CRs need complex receiver front end architectures.

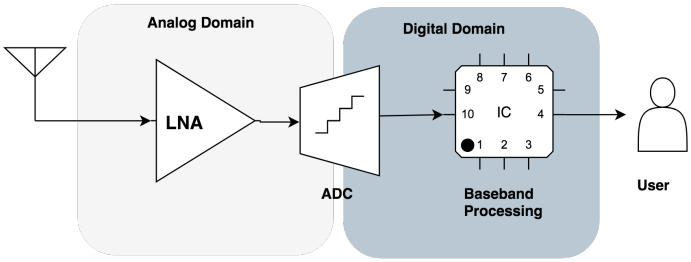

Fig. 6. Ideal receiver for CRs.

3.1.1.1 Heterodyne architecture: Fig. 7 shows a classical architecture of a receiver using heterodyne structure. In the heterodyne receiver, the received signal first passes through a BPF. The further degraded signal from the BPF passes through an LNA for amplification. The amplified signal gets downconverted by a mixer and LO. The downconverted baseband signal passes through a LPF and an AGC to avoid aliasing and clipping issues. The ADC converts the analog signal to the digital domain. The heterodyne receiver could also have an in-phase(I) and quadrature (Q) branches after the mixer. The heterodyne receiver is excellent in terms of adoption of different protocols and provides satisfactory selectivity and sensitivity. However, the heterodyne receiver does not solve the image problem. The image problem occurs during the downconversion process. The implementation of image rejection filters solves the image problem in the receiver front end. The heterodyne receivers also contain many analog components such as BPFs and image rejection filters to improve performance [9]. Therefore, the power consumption of the heterodyne receiver is high.

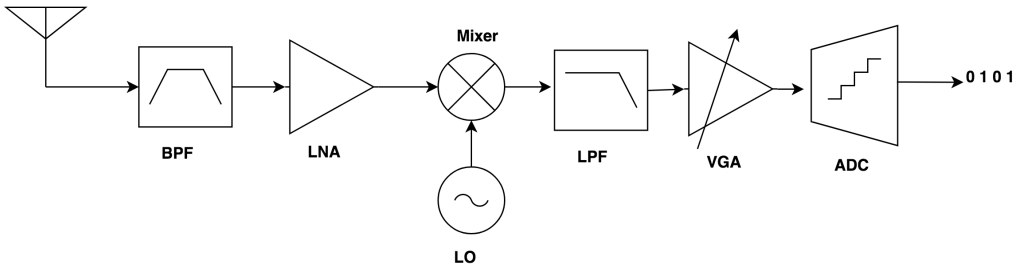

Fig. 7. Simple heterodyne receiver architecture design.

3.1.1.2 Zero-IF architecture: Zero-IF stands for Zero Intermediate Frequency. Zero-IF receiver architecture uses fewer analog components than heterodyne architecture. Hence, the power consumption of the Zero-IF receiver is lower [9]. As shown in Fig. 8, the received signal passes through a BPF and then an LNA similar to the heterodyne receiver. The downconversion to I/Q branch is where the Zero-IF receiver differs from the heterodyne receiver. In the Zero-IF receiver, the downconversion takes place only once unlike the heterodyne receivers. Flicker noise and DC offset are major disadvantages of Zero-IF receivers.

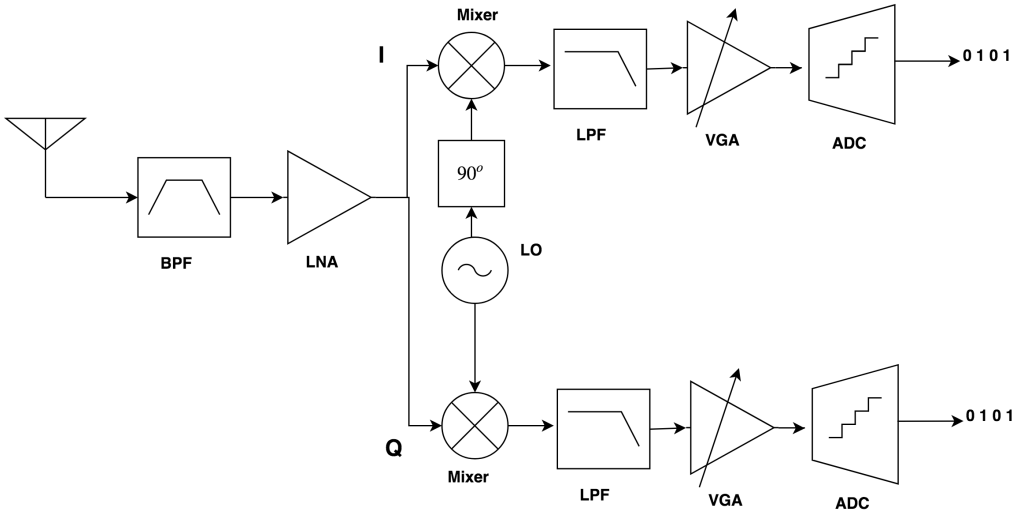

Fig. 8. Zero-IF receiver architecture design.

3.1.1.3 Other architectures: Digital low-IF receivers are another type of receiver design that combines the design ideas of the heterodyne receiver and the Zero-IF receiver. The additional down conversion step is added in the digital domain on top of the Zero-IF design as shown in Fig. 8. However, the image frequency problem persists. Hence, the digital low-IF receiver requires more analog components for downconversion [9]. Bandpass sampling receivers are useful when the sampling rate of the ADC is low. The bandpass sampling receivers take advantage of the fact that the under-sampling of a bandpass spectrum generates duplicates of the spectrum in the low-pass region. The BPF filter used after the antenna must be designed with minimum gain loss for the receiver to work efficiently. The power consumption of the bandpass sampling receiver is low since the required sampling rate of the ADC is low.

3.1.2 Receiver Front End Components Analysis

The receiver front end consists of many circuit blocks that have different requirements of power. This section provides the information on the previous work done to derive a model for the power consumption of receiver front end circuit blocks.

Analog filters used in the receiver front end for CRs need to be reconfigurable or tunable to cover a wide range of frequency band. The low power consumption of a tunable analog filter leads to degraded receiver speed [9]. Hori et al. [10] present a tunable wideband analog filter. The figure of merit (FoM) is a model to compare a new or upcoming model to the existing ones. The efficiency of a wideband analog filter based on FoM is [10]

$$\text{FoM} = \frac{P_{total}}{N \cdot f_c \cdot \text{SFDR} \cdot N^{4/3}} \tag{6}$$

where P_{total} is the full power consumption of the wideband analog filter, N is the total number of zeros and poles of the filter, f_c is the cut-off frequency, and SFDR stands for spurious-free dynamic range.

Gianni et al. [9] provide information on many analog filters used in receiver front end. The power consumption of the analog filter depends on the parameters like complementary metal–oxide–semiconductor (CMOS) technology, the filter order, and bandwidth. In Fig. 9, the data of the power consumption and the bandwidth of the filter is plotted. The line in Fig. 9 is the best estimate of the linear relationship between the power consumption and analog filter bandwidth. The mathematical representation of the line is

$$P_{filter} = 0.1976 \cdot W + 13.389 \tag{7}$$

where P_{filter} is the power consumed by the analog filter in milliwatt and W is the bandwidth of the analog filter.

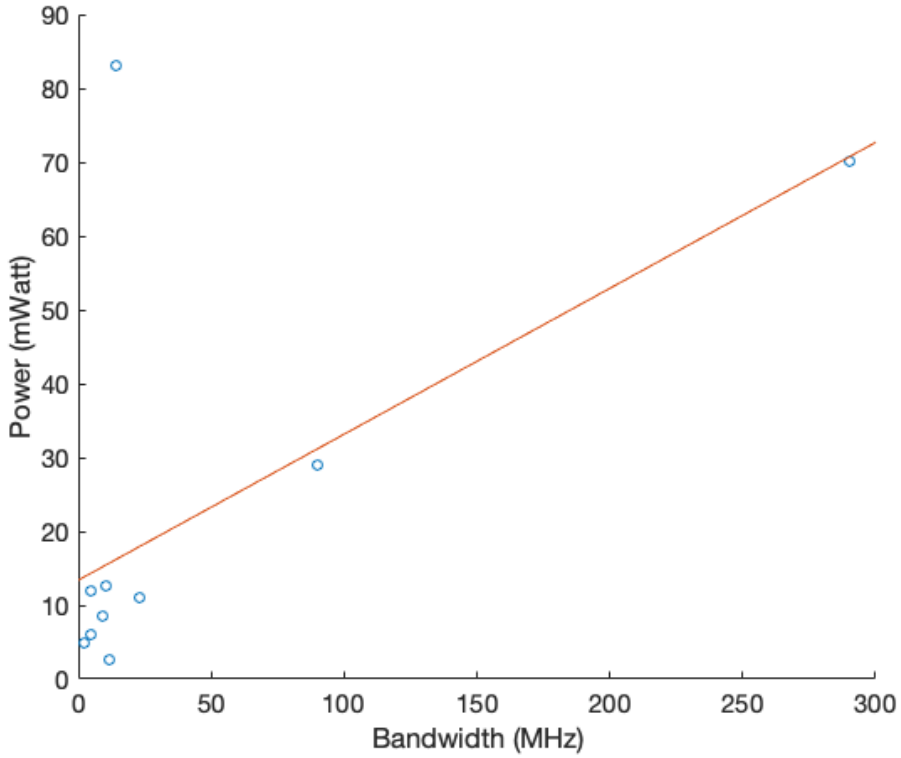

Fig. 9. Linear model of analog filters.

Based on (7), there is a linear relationship between the power consumption and the bandwidth. Hence, the power loss of the analog filter increases with the bandwidth. The linear model in (7) is based on minimal data. Hence, the model for the analog filter cannot be generalized.

A low-noise amplifier amplifies a weak signal received through an antenna. The design and the operation of the LNA depend on the critical parameters like IIP3, bandwidth, noise figure (NF), and gain. In [11], a relationship between the power consumption of a two-stage LNA and the critical design parameter is shown as

$$P_{\mathrm{LNA}} = 2\sqrt{G_{tot} \cdot k_1 \cdot k_2 \cdot \mathrm{IIP3}_1 \cdot \mathrm{IIP3}_2} \tag{8}$$

where G_{tot} is the total gain of the amplifier, k_1 and k_2 are the technical parameters, $\mathrm{IIP3}_1$ and $\mathrm{IIP3}_2$ are the IIP3 values of the two amplifier stages.

The noise figure of a circuit block is the ratio of the input SNR to output SNR. The degradation of the input signal's SNR by a receiver circuit block is analyzed using the NF.The design of LNA shown in [11] has a trade-off between the parameters like the gain, NF and IIP3. The IIP3 and NF are small for a high gain amplifier.

Lolis et al. [12] propose a model for computing the power consumption of the LNA based on the high-level parameters. The model to determine the power consumption of an LNA includes a FoM. The relation between the power consumption of an LNA and high-level parameters is

$$P_{\mathrm{LNA}} = \frac{G \cdot \mathrm{IIP3} \cdot f_c}{F_{\mathrm{LNA}} \cdot \mathrm{FoM}_{\mathrm{LNA}}} \tag{9}$$

where G is the gain of the LNA, f_c is the center frequency of the input signal, $\mathrm{FoM}_{\mathrm{LNA}}$ is the figure of merit for LNAs, and F_{LNA} is the operational frequency of the LNA.

Mixers are a critical part of the receiver front end. The mixers are usually placed after the LNA as shown in Fig. 7. The outputs of LNA and LO are fed into the mixer to

perform a non-linear operation. The mixer multiplies input signals. The multiplication process creates outputs at the sum of the input signal frequency and the difference of the input signal frequencies as shown in Fig. 10. In Zero-IF receiver design, the frequency of the LO is the same as the frequency of the LNA to directly down-convert the signal to baseband.

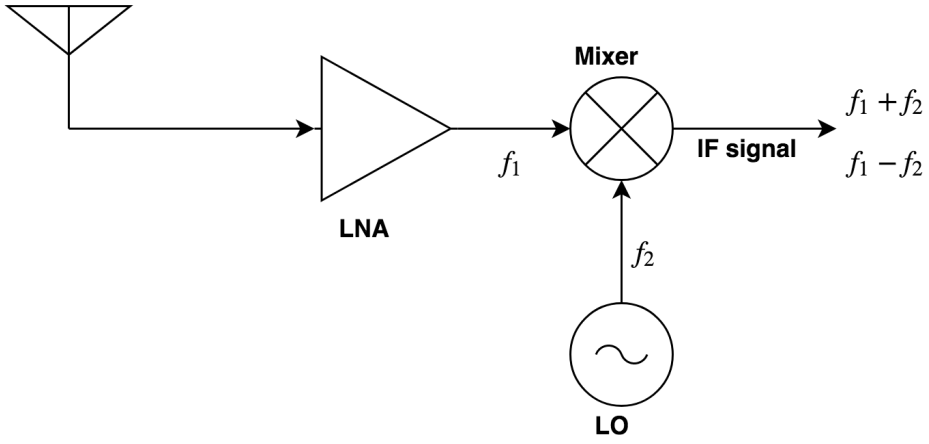

Fig. 10. Role of a mixer at receiver front end.

The power consumption of the mixer depends on the design parameters such as IIP3, conversion loss, NF, and dynamic range. Due to non-linear operation of a mixer, IIP3 is a crucial parameter to test the performance. The output signal from passive mixer usually suffers from the loss. The dynamic range of the mixer increases with the SNR. The NF determines the noise added by the mixer to the input signal. The NF of the mixer should be as low as possible since the noise added by the mixer is not removable.

A phase-locked loop is used to generate reference frequencies in the receiver front end. A phase-locked loop is a system with negative feedback. A voltage-controlled oscillator (VCO) and comparators are integral parts of a PLL. High power consumption and low tuning speed are the main disadvantages of a PLL [11].

The local oscillator refers to a device that can generate stable reference frequencies. A phase-locked loop can be used as a LO to generate reference frequencies required in the

receiver front end. The LO generates random phase variations that are known as phase noise. Hence, the phase noise is a critical parameter in determining the performance of a LO. The phase noise decreases with an improvement in the performance of the oscillator [13]. The NF of the LO is directly related to the phase noise [11]. The phase noise and the power consumption of a LO have a reciprocal relationship. Hence, reducing the power consumption means increasing the phase noise and NF. Gao et al. [11] designed a model for the power consumption of an injection-locked oscillator(IJLO). As per the model, the relationship between the power consumption of the IJLO and high-level parameters is

$$P_{\mathrm{IJLO}} = C \cdot \left(\frac{R}{L}\right)^3 \cdot \mathrm{NEF} \cdot \frac{k \cdot T}{S_\phi} \cdot \frac{\omega_c^2}{\mathscr{Q}^2 \cdot (\Delta\omega^2)} + k \cdot G \cdot \mathrm{IIP3} \tag{10}$$

where C represents capacitance, L represents inductance, R represents resistance, k is the Boltzmann constant, $\mathscr{Q}$ is the quality factor, NEF is the Noise Excess Factor, T is the temperature in Kelvin, $\Delta\omega$ is the offset frequency, and S_ϕ is the noise power density.

An analog-to-digital converter is the most dominant part of the receiver front end in terms of power consumption. The critical parameters for the ADC are the ENOB, dynamic range, and sampling rate. There are many architectures of the ADC. Flash, pipelined, integrating, sigma-delta are some of the known architecture of the ADC. The flash ADC uses comparators to convert the input analog signal to bits. The flash ADC is also the fast as the conversion from analog to digital bits happens in one clock cycle. For N bit conversion, the flash ADC requires $(2^n - 1)$ comparators. Hence, the number of comparators needed for high-resolution flash ADC is very high. The size and power consumption both increase exponentially for high N flash ADC. For high-speed applications, flash ADC is a good choice.

The pipelined ADC divides the analog to digital conversion task into several stages. Due to multiple stage design, it is possible to realize a pipeline ADC with higher

resolution then flash ADC. However, the speed of the conversion in pipelined ADC reduces. Integrated ADC uses an integrator circuit to do analog to digital conversion. The integrated ADC can get up to 12-16 bit resolution. However, the integrated ADC is slower than the pipelined version. The sigma-delta ADC uses noise shaping and oversampling methods to achieve high resolution.

Murmann and Boris [14] collected the data on the power consumption and the sampling rate for many different ADC designs. In Fig. 11, the plot of the power consumption of various ADCs versus the sampling rate of the ADC is shown.
From Fig. 11, there is no clear relationship between the power consumption and the sampling rate of the ADC. Besides, the power consumption of the ADC cannot be modeled solely based on the sampling rate as the ENOB, SQNR, and SNR are the other key factors to influence the ADC performance and power consumption.

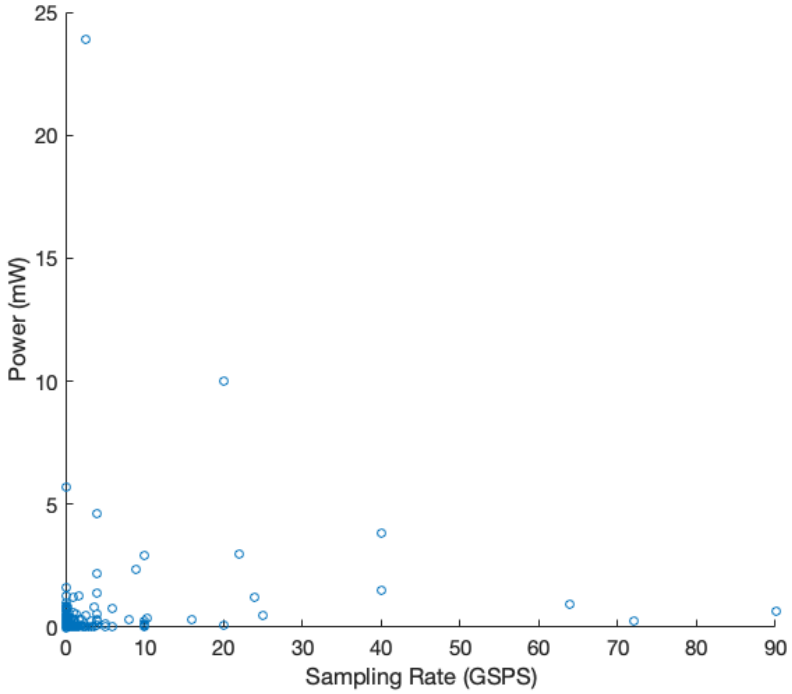

Fig. 11. ADC power versus sampling rate survey.

Heydari [15] proposed a wideband receiver power consumption model. In the model, the power consumption of an ADC depends on parameters like reference voltage, number of bits, and clock frequency. The power consumption model is

$$P_{ave} = 2^{N-2} \cdot \left(\gamma^{-1} \cdot C_S \cdot V_{ref}^2 \cdot f + (1-\gamma)^{-1} \cdot V_{DD} \cdot I_{DD} \right) \tag{11}$$

where N is the resolution of the ADC, C_S is the equivalent switched capacitance of each comparator, V_{ref} is the reference voltage for the ADC conversion, f is the clock frequency of the comparator, γ is the fraction of the clock period used for comparison, V_{DD} is the supply voltage, and I_{DD} is the DC current drawn from the supply voltage.

3.2 One-Band Spectrum Sensing Methods

The primary goal of the one-band spectrum sensing is to detect an empty band. The $\mathscr{H}_0$ hypothesis suggests that the received signal is the PU signal with noise, and the $\mathscr{H}_1$ hypothesis suggests that the received signal is only noise. A one-band spectrum sensing model with $\mathscr{H}_0$ and $\mathscr{H}_1$ hypothesis can be expressed as

$$\begin{aligned} \mathscr{H}_0 : &\quad x(n) = s(n) + v(n) \\ \mathscr{H}_1 : &\quad x(n) = v(n) \end{aligned} \tag{12}$$

where $x(n)$ represents the signal detected at the receiver, $s(n)$ is the PU signal, $v(n)$ is the additive white Gaussian noise (AWGN) signal.

Any method based on the hypothesis shown in (12) can be evaluated with the probability of detection (P_d) and the probability of false alarm (P_f).

$$P_d = p(\mathscr{H}_1 | \mathscr{H}_1) \tag{13}$$

$$P_f = p(\mathscr{H}_1 | \mathscr{H}_0) \tag{14}$$

3.2.1 *Energy Detector*

In the energy detection method, the received signal is converted to an energy signal. The sum of energy samples is then compared to a threshold to decide the presence or absence of a PU [16], [17].

$$T(x) = \sum_{k=1}^{M} |X(k)|^2 \tag{15}$$

Where $T(x)$ is the total energy of M samples, and $X(k)$ represents the fast Fourier transform (FFT) of the received samples. $|.|$ is the operation of taking absolute value of a complex number.

As shown in Fig. 12, the samples from the RF front end are converted into the frequency domain using a FFT algorithm. To accurately find empty bands, M samples of the received signal per band is accumulated as shown in (15). The sum of accumulated received samples is then compared to a threshold to decide on $\mathscr{H}_0$ or $\mathscr{H}_1$ hypothesis.

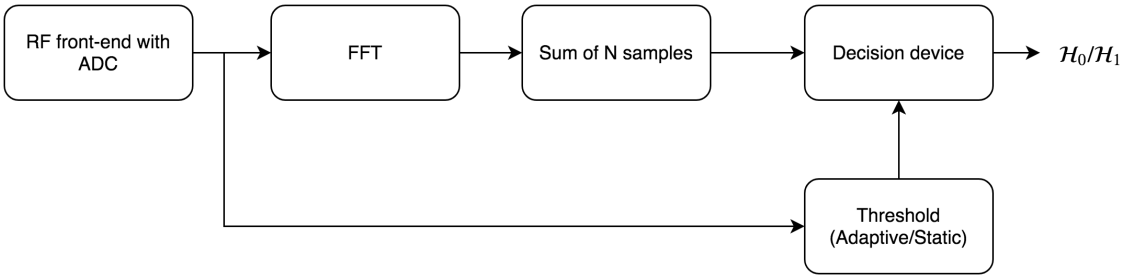

Fig. 12. Energy detector.

$$T(x) \gtrless T_0 \tag{16}$$

The $T(x)$ is compared to a operating threshold (T_0) to decide the appropriate hypothesis as shown in (16).

The performance of the energy detection method heavily depends on the selection of T_0. The value of T_0 can be static or dynamic. An optimal value of T_0 can increase the performance of the energy detection method dramatically [18]. The energy detection method does not depend on the prior information of the received signal. At a low SNR, the performance of the energy detection method is poor [19].

The energy detection method could be handy when the frequency of the spectrum sensing is low. There is an opportunity to optimize the energy loss of the receiver front end because the resources are not used continuously to decide the hypothesis. The number of sample M can also be optimized such that the receiver front end resources are used with a minimum amount of time to get optimal performance [20].

3.2.2 Cyclostationary Detector

$$R_x(\tau) = E[x(t) \cdot x(t+\tau)] \tag{17}$$

$$S_x(\alpha, \tau) = \sum_{\tau=-\infty}^{\infty} R_x(\tau) \cdot e^{-j2\pi\alpha\tau} \tag{18}$$

Where τ is the period of the received signal, $E[.]$ is the expectation, S is the cyclic spectral density (CSD), and α is the cyclic frequency.

Cyclostationary method exploits the repetitive nature of the input signal to decide the hypothesis in (12). In some cases, the PU signal includes data redundancy to get more protection against noise ambiguity at the receiver [21]. The method of detecting PU using the cyclic redundancy in the received signal is called cyclostationary detection [19]. As shown in Fig. 13, the cyclostationary detector uses the second order statistics like the correlation of the received signal to decide the hypothesis in (12). The correlation of the input signal is formulated in (17).

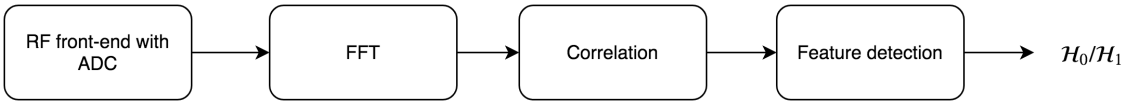

Fig. 13. Cyclostationary detector.

Based on the CSD shown in (18), the updated hypothesis to detect the presence of the PU can be shown as

$$\begin{aligned} \mathscr{H}_0: &\quad S_x(\alpha,\tau) = S_s(\alpha,\tau) + S_v(\alpha,\tau) \\ \mathscr{H}_1: &\quad S_x(\alpha,\tau) = S_v(\alpha,\tau) \end{aligned} \tag{19}$$

The cyclostationary method depends on the prior information about PU's data. The performance of the cyclostationary method is superior to the energy detector method since the second order statics distinguish the PU signal from the noise. An optimized cyclostationary method is also available where complexity and sensing time is an issue in implementation [22].

The cyclostationary method depends heavily on the second order statics which complicates the post-processing of the signal. The autocorrelation requires two cycles of the input signal. The sensing time increases due to the compilation of two cycles of the input signal. From the energy consumption perspective, the cyclostationary method provides less optimization than the energy detection method.

3.2.3 Matched Filter Detector

$$T(x) = \sum_{n=1}^{M} x(n) \cdot x_p^*(n) \tag{20}$$

where x_p^* is the complex conjugate of the saved pilot data of the PU, and M is the total number of samples collected.

The matched filter detection depends on the knowledge of the pilot data transmitted by the PU [23], [24]. The known pilots are used to compute the test statistics. The comparison of the test statistics with the threshold determines the result. As shown in Fig. 14, the received signal is multiplied with the known pilots to generate the test statistics. The result of the test statistics is then used to decide the hypothesis in (12) by comparing the test statistics to the threshold.

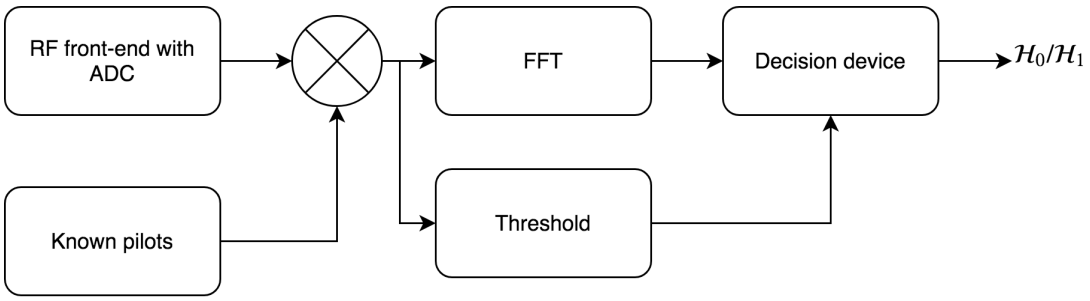

Fig. 14. Matched filter detector.

As shown in (20), the test statistics can be calculated using the complex conjugate of the known pilots of the PU. The calculated test statistic is then compared to a threshold as shown in (16) to decide the correct hypothesis.

The matched filter detection may perform better than the cyclostationary detection method since the determination of band status can be done faster. Similar to the energy detection method, the performance of the matched filter detection method depends on the selection of the threshold. Dynamic selection of the threshold makes the matched filter method optimal.

In terms of energy consumption of the RF front end, the matched filter detection method could be beneficial for a small M. Due to the perfect knowledge of pilots of the PU, the fast detection of a full band is possible. Fast detection saves the receiver front end energy. However, the assumption that the information about the PU signal is available is not practical in most situations.

3.2.4 Other Methods

One-band detection can also be done using the covariance method. In the covariance method, a model of the received samples is used in conjunction with the singular value decomposition technique to decide the hypothesis in (12) [25], [26]. The process of determining the hypothesis includes the calculation of the eigenvalues along with a threshold. Similar to energy detection, the threshold limits the detection performance. The assumption for the covariance based method includes no prior knowledge of the PU. However, the computational complexity is very high since the method requires complex matrix manipulation. In terms of energy consumption of the receiver front end resources, the covariance method is as efficient as the energy detector method. The extra computation complexity makes the covariance based detection method inefficient compared to the energy detection method.

Due to recent advancement in the field of machine learning, many machine learning based spectrum sensing algorithms are proposed. In [27], [28], the authors have posted the spectrum sensing problem as supervised and unsupervised classification. Based on the classifier, a vector of probability is inferred to decide the state of the frequency band in question. The primary goal of the machine learning based spectrum sensing algorithms is to detect the pattern of the PU signal and use the detected patterns to decide the status of the band. The detection performance of machine learning based methods depends heavily on computational complexity. The IoT based CR does not have high computational complexity to train and save large machine learning models continuously. Besides, the time to train the model and the classification delay are other parameters that are taken into account while deciding the detection performance of the machine learning based methods. The receiver front end resources are heavily used during the model training. The receiver front end resources lose energy while the training is running. Hence, machine learning based methods may not be a realistic option in a restrictive energy environment.

3.3 Multi-Band Spectrum Sensing for Primary Detection

Multi-band spectrum sensing divides a large band into B small sub-bands $(s_1, s_2, s_3, ..., s_B)$ as shown in Fig. 15, and finds the PU present in the spectrum. In multi-band spectrum sensing scenario, the hypothesis $\mathscr{H}_0$ is defined as all the B sub-bands are empty. While the hypothesis $\mathscr{H}_1$ is defined as the full bands that belong to the set of PU bands L and empty if the band does not belong to the set L. The size of the set L is the same as the total number of the PU bands. The size of set L is B when all the bands are filled with PU. The multi-band hypothesis is formed as

$$\begin{aligned} \mathscr{H}_{0,i}: \quad & \mathbf{x}_i(n) = \mathbf{v}_i(n) && i = 1 \ldots B, \\ \mathscr{H}_{1,i}: \quad & \mathbf{x}_i(n) = \mathbf{s}_i(n) + \mathbf{v}_i(n) && i \in L \\ & \mathbf{x}_i(n) = \mathbf{v}_i(n) && i \notin L \end{aligned} \tag{21}$$

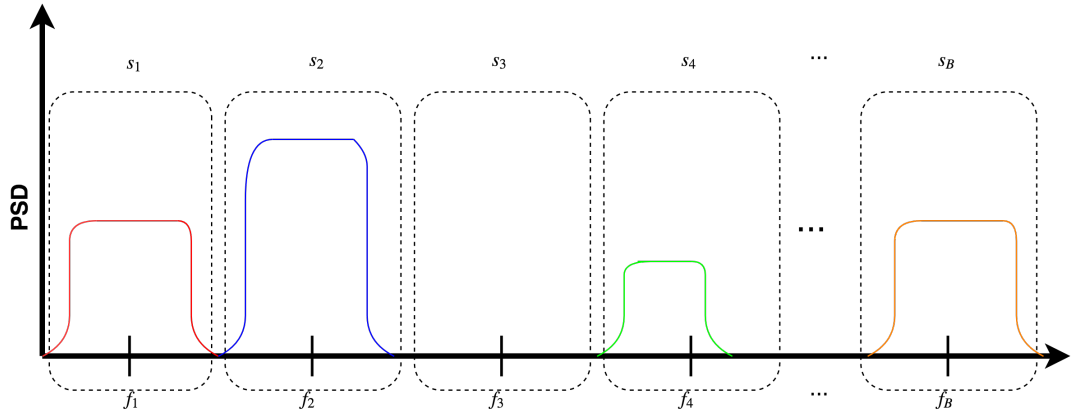

Fig. 15. Multi-band spectrum sensing.

$$T(x_i) \gtrless T_{0,i} \tag{22}$$

The performance matrix of a multi-band spectrum sensing algorithm is simplified into (22) if there is no correlation between the sub-bands [29]. Each sub-band in the spectrum is compared to an operating threshold to decide the presence of a PU. A general performance matrix to incorporate the detection of multiple bands is discussed in detail in Chapter 6.

3.3.1 Serial Detector

In the serial detection method, the sub-bands are scanned one by one to find PUs. The receiver front end needs to have some reconfigurable resources to search multiple bands serially. The BPF and LO are adjustable circuit blocks of the receiver front end [29].

3.3.1.1 Adjustable BPF: With an adjustable BPF, the receiver front end can sense sub-bands one by one. After tuning the BPF to a specific sub-band, one-band spectrum sensing methods can determine the activity of the PU. The design of the wideband receiver with configurable BPF is challenging [30]. Hence, the implementation of the adjustable BPF is expensive. A wideband receiver also requires a wideband ADC, and the wideband ADC uses more power than a narrowband ADC. Therefore, the receiver front end consumes more energy with the adjustable BPF.

3.3.1.2 Tunable LO: A local oscillator generates the reference frequency of interest. The reference frequency from the LO helps down-convert a sub-band located at a high frequency. Since the LO downconverts the signal, the output signal is a lowpass signal. Hence, a low sampling rate ADC is required. Due to the low sampling rate ADC, the receiver front end consumes less energy. The downside of the tunable LO configuration is the slow speed of tuning. The speed of the spectrum sensing is limited by the speed of the tunable LO.

3.3.2 Wavelet Detector

The wavelet-based detection method is useful when the locations of the sub-bands are not known [31], [32]. The location of the sub-bands are shown in Fig. 15 as $f_1, f_2, \ldots, f_B$.

As shown in Fig. 16, the incoming signal is converted into the PSD using the FFT algorithm. The wavelet transform operates on the PSD of the received signal. The transformed signal is used to detect any singularities [33]. The singularities help identify edges of sub-bands.

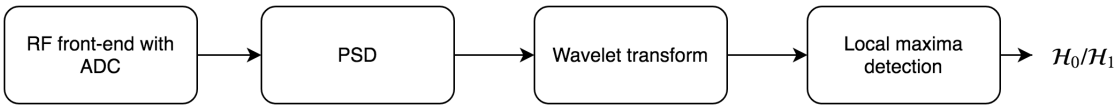

Fig. 16. Wavelet detector.

The wavelet-based sensing can be energy efficient as the receiver front end needs to collect only a limited number of sample. However, to identify the sub-band edges accurately, the computational complexity of the wavelet-based detection method increases significantly.

3.3.3 Joint Detector

In multi-band spectrum sensing, the joint detection method performs the one-band spectrum sensing process for multiple bands in parallel [34]. As shown in Fig. 17, the input signal is converted to parallel. After the conversion from serial to parallel, the signal is transformed into the frequency domain PSD using the FFT algorithm. The PSD of each band is used to detect full or empty band using one-band spectrum sensing methods discussed in Chapter 3.2. Different thresholds decide the activity of a PU at each arm of the joint detector. Hence, the joint detection method provides a vector of thresholds for the sub-bands. Due to the different threshold for each sub-band, the efficiency of the joint detection algorithm increases [35]. At each parallel stage, the one-band spectrum sensing method can be different. However, the use of many one-band spectrum sensing methods in parallel increases the computational complexity of the receiver. The energy consumption of the joint detection is high because the high number of samples required to do parallel detection.

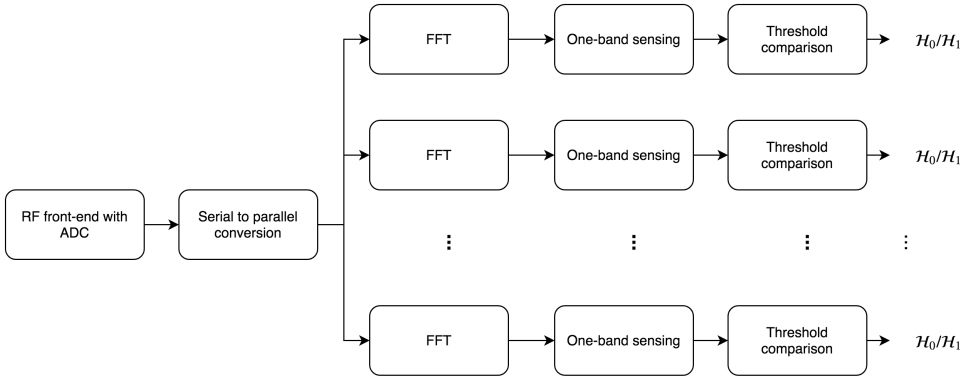

Fig. 17. Joint detector.

3.3.4 Filter Bank-Based Detector

The filter bank-based method requires a bank of discrete BPFs to convert the received signal into many different sub-bands [36], [37]. As shown in Fig. 18, sub-bands at the output of BPFs are processed using one-band spectrum sensing methods. Since the filter bank increases the complexity of the receiver by requiring many hardware changes, the filter bank-based method consumes more energy [29].

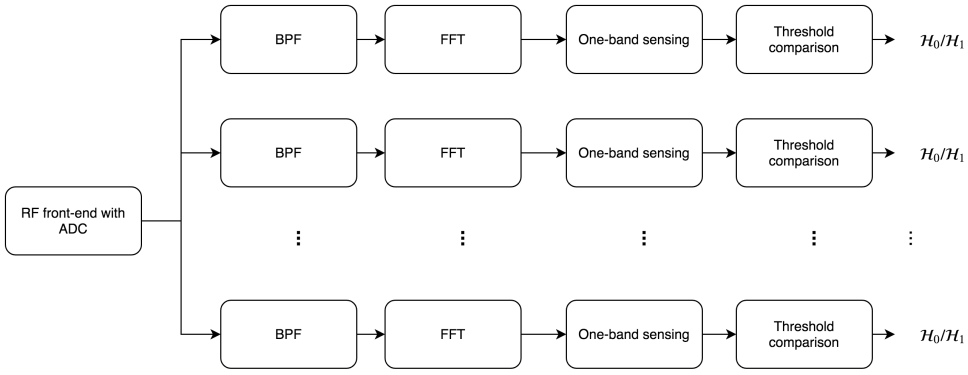

Fig. 18. Filter bank-based detector.

$$T(x_i) = \sum_{k=1}^{M} |X_i(k)|^2 \qquad i = 1 \ldots B \qquad (23)$$

where $X_i(k)$ is the Fourier transform of the input signal $x_i(n)$ for ith sub-band. The test statistics for each sub-band using the energy detector is shown in (23).

3.3.5 Other Detectors

Compressive spectrum sensing uses a sub-Nyquist sampling rate to reconstruct the received signal. If the PU signal is sparse in the frequency domain, the signal in the frequency band can be detected using a lower sampling rate than the sampling rate suggested by Nyquist theorem [38], [39]. For example, to correctly construct the spectrum at 1 GHz, the sampling rate needs to be at least 2 GHz as per Nyquist theorem. However, the signal can be reconstructed using sub-Nyquist sampling rates if the signal at 1 GHz is sparse, and the spectrum is scarce. The lower sampling rate reduces the sampling rate requirement of ADC; therefore, the energy consumption of the receiver front end may also be relaxed. In a restrictive energy environment, the compressive sensing method could be handy. Due to the lower sampling rate, the received signal suffers from degraded SNR. Also, the non-linearities in the receiver front end components like mixers and amplifiers affect the sub-Nyquist sampling negatively.

Knowledge of signal propagation angle used by the PU also opens up a new opportunity to do multi-band spectrum sensing. Spectrum sensing based on the information of propagation angle is called angle spectrum sensing. Due to the deployment of multiple input multiple output (MIMO) and beamforming systems, there could be a place where SU can use the same frequency band as PU if the frequency band used by the SU does not cross the propagation angle of the PU [40]. The concept of angle spectrum sensing is beneficial in terms of energy saving as the spectrum bands can be used by both PU and SU simultaneously.

Blind spectrum sensing is another type of multi-band spectrum sensing where no information about the PU signal is required. The blind spectrum sensing is the case in many scenarios and environments due to the increase in the frequency domain traffic [41]. The energy consumption of the receiver front end depends on the spectrum activity. If the spectrum is full with high SNR signals, the energy expenditure of the receiver front end is high.

4 SYSTEM MODEL

In the CR environment, the energy sources are often limited. Chapter 4 defines the mode of operations of the CR. Utilizing tools from recent works, a model to calculate and analyze the energy consumption of a receiver front end is discussed in Chapter 4.2.

4.1 Receiver's Operation Status

In the communication system, there are times when the receiver is not receiving any data nor doing the spectrum sensing. Hence, the receiver changes status based on the operation. The receiver holds one of the four statuses: 1) transient; 2) active; 3) sleep; and 4) ideal. In active status, the receiver is either receiving the data or scanning the spectrum to find empty bands. In ideal status, the power to the receiver is on, but the receiver is neither receiving the data nor scanning the spectrum for empty bands. In transient status, the receiver is transitioning from one status to another status, and the active components of the circuit are getting settled into the new status. In sleep status, the power to the receiver front end is turned off. The power consumption in the active status is the highest since all of the components of receiver front end are running. The power consumption of the ideal status is higher than the sleep status but lower than the active status. All four statuses of the receiver are shown in Fig. 19. The power consumption of the transient status may not be as smooth as shown in Fig. 19 as the transient power consumption in RF integrated circuits depends on dose rate [42].

The total operating time, T, of the receiver is defined as

$$T = T_{Active} + T_{Idle} + T_{Transient} + T_{Sleep} \tag{24}$$

Based on (24), the total energy consumption of the receiver front end is

$$E_{tot} = P_{Active} \cdot T_{Active} + P_{Idle} \cdot T_{Idle} + P_{Transient} \cdot T_{Transient} + P_{Sleep} \cdot T_{Sleep} \tag{25}$$

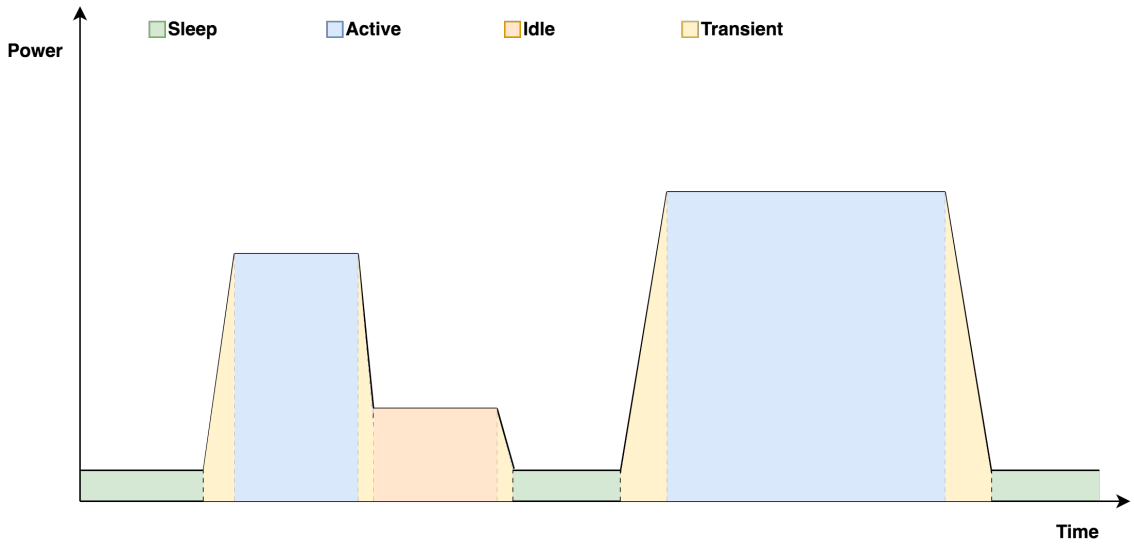

Fig. 19. Receiver operation status monitor.

The energy consumption during the idle and sleep status is very low compared to the energy consumption of the active status [8]. Since energy consumption during the transient time is unstable and lower than the idle status, the energy consumption of the transient state is also ignored.

The energy consumption of the active status can further be broken down into spectrum sensing mode and data receiving mode as

$$E_{Active} = E_{sns} + E_{data}$$
$$E_{Active} = P_{sns} \cdot T_{sns} + P_{data} \cdot T_{data} \tag{26}$$

Since we are only interested in energy loss during spectrum sensing, energy loss during data receiving is ignored. Hence, the total spectrum sensing energy loss is

$$E_{sns} = P_{sns} \cdot T_{sns} \tag{27}$$

4.2 Receiver Front End Energy Model

Fig. 20 shows a generalized structure of receiver front end architecture with the critical components like an LNA, a splitter, multipliers, LPFs, and ADCs. The receiver is of the quadrature type which is widely popular in software defined radios (SDRs) [9]. Outputs of in-phase and quadrature ADCs are transferred to the digital processing devices such as field-programmable gate arrays (FPGAs) to generate a spectrum using the FFT algorithm. The spectrum is then analyzed using various spectrum sensing algorithms to decide the state of the band.

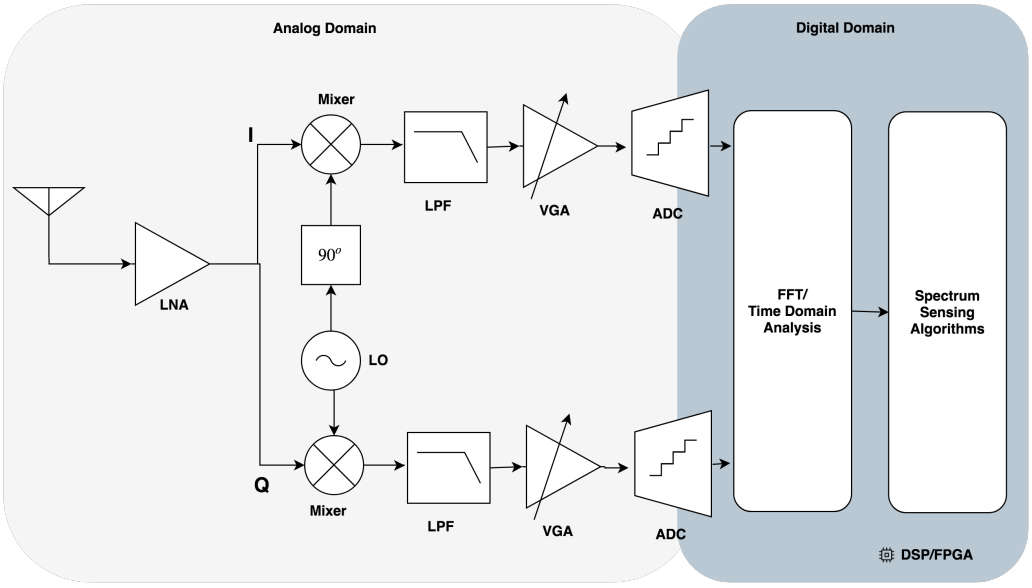

Fig. 20. Receiver front end architecture for energy model.

To build a flexible CR that can work with wideband signals, the VGA needs to be compatible with the wideband signal. The power consumption of the VGA depends on key high-level parameters such as the SNR, CMOS technology, and phase noise [43]–[45]. If the phase noise requirements are relaxed, then for a given 3-dB bandwidth and input voltage signal range, the power consumption of the VGA depends on the design of the CMOS circuit and power supply.

The power consumption of the LNA calculated in (9) also includes the power consumption of the ADC. The power consumption of the ADC used with the LNA is assumed to be constant. Therefore, the power consumption of the reconfigurable LNA can be calculated using (9) only if the ADC power consumption is considered constant. Since there is no strict requirement of the NF and gain, the power consumption of the LNA can be assumed constant.

The splitter and mixers are the components of the receiver front end whose power consumption depends on the parameters such as the NF and IIP3. The power consumption of the mixers and splitter should be as low as possible due to the power constraint requirements of the IoT devices. There are ways to reduce the power consumption of the mixers and splitters by putting constraints of the design parameters like phase noise and supply voltage [46].

The power consumption of LPFs does not depend on the input signal frequency. The power of the LPF may increase with an increase in the bandwidth of the filter depending on the design. For a fixed bandwidth, the power consumption of a LPF does not change significantly.

The ADC performance depends on the parameters like the input signal swing, speed of the analog to digital conversion, number of bits, and quantization noise. A system level model of the ADC can be derived by dividing the ADC model into two parts [47]. The first component is the comparator and the second component is the digital circuit that converts outputs of the comparators to the digital numbers [47]. The ADC used in this work is a high-speed Nyquist rate ADC. The power model of the ADC does not depend on the actual implementation method of the ADC such as flash and pipeline [47]. A model for the power dissipation of an ADC is [8]

$$P_{\text{ADC}} = \frac{V_{dd}^2 \cdot L_{min} \cdot \left(F_{sample} + F_{signal}\right)}{10^{(-0.1525 \cdot N_1 + 4.838)}} \tag{28}$$

where V_{dd} is the ADC supply voltage, L_{min} is the size of the CMOS technology node, F_{sample} is the frequency of the comparators, F_{signal} is the frequency of the signal, and N_1 is the effective bit resolution.

The bit resolution based on the quantization noise of the ADC is also known as effective number of bits. According to Cui et al. [48], the resolution N_1 is a function of the SQNR and PAPR as

$$N_1 = \frac{\mathrm{SQNR\,(dB)} + \mathrm{PAPR\,(dB)} - 4.77\,\mathrm{(dB)}}{6.02} \tag{29}$$

If we assume that the signal frequency F_{signal} is half or less of the F_{sample} as per Nyquist theorem, (28) can be written as [48], [49]

$$P_{\mathrm{ADC}} = \frac{V_{dd}^2 \cdot L_{min} \cdot F_{sample} \cdot \frac{3}{2}}{10^{(-0.1525 \cdot N_1 + 4.838)}} \tag{30}$$

Hence, the power consumption of the ADC depends on the signal parameters such as the SNR, PAPR, and F_{sample}. The power consumption of the multipliers and splitter is very low and does not vary with the vital signal parameters; therefore, the power consumption of the multipliers and splitter is ignored.

$$P_{Total} = P_{\mathrm{LNA}} + P_{\mathrm{LO}} + 2 \cdot P_{\mathrm{LPF}} + 2 \cdot P_{\mathrm{VGA}} + 2 \cdot P_{\mathrm{ADC}}$$

Since the power consumption of the BPF, LPF, LNA and VGA does not depend on the signal parameters like the SNR and F_{sample}, the power consumption of these blocks can be assumed constant.

$$P_{Other} = P_{\mathrm{LNA}} + P_{\mathrm{LO}} + 2 \cdot P_{\mathrm{LPF}} + 2 \cdot P_{\mathrm{VGA}}$$

Therefore, the total power loss of the receiver front end is

$$P_{Total} = P_{Other} + 2 \cdot P_{\mathrm{ADC}} \tag{31}$$

Based on (27) and (31), the energy consumption based on the spectrum sensing time can be calculated as

$$E_{Total} = (P_{Other} + 2 \cdot P_{\mathrm{ADC}}) \cdot T_{sns} \tag{32}$$

$$E_{Total} = E_{Other} + 2 \cdot E_{\mathrm{ADC}} \tag{33}$$

The total energy consumption by the RF front end is in terms of the spectrum sensing time, SNR, PAPR, and F_{sample}. The energy consumed by the other component is constant. The sensing time depends on the sampling frequency, F_{sample}, and number of samples per band, M.

$$T_{sns} = \frac{M}{F_{sample}} \tag{34}$$

From (30) and (34),

$$E_{\mathrm{ADC}} = \frac{V_{dd}^2 \cdot L_{min} \cdot M \cdot \frac{3}{2}}{10^{(-0.1525 \cdot N_1 + 4.838)}} \tag{35}$$

Therefore the energy consumption of the ADC also depends on the number of samples per band, M. Combining (33) and (35) gives the energy consumption formula for the receiver front end.

$$E_{Total} = E_{Other} + \frac{V_{dd}^2 \cdot L_{min} \cdot M \cdot 3}{10^{(-0.1525 \cdot N_1 + 4.838)}} \tag{36}$$

The energy consumption model derived in (36) applies to the receiver front end architecture shown in Fig. 20. The model for energy consumption of an ADC shown in (35) can also be applied to the parallel energy detectors shown in Chapters 3.3.3 and 3.3.4.

5 A FRAMEWORK FOR THE ANALYSIS OF MULTI-BAND SPECTRUM SENSING

In the multi-band spectrum sensing problem, the main goal is to estimate multiple empty bands locations in the multi-band spectrum. Sirkeci and Collins [50] propose a framework to find PUs in the multi-band spectrum sensing scenario. In this section, a modified version of the multi-band framework in [50] is used to find empty bands. The assumption is that the spectrum is divided into multiple bands, and the empty bands occupy a subset of these bands. In the following, the maximum number of available bands (B) and the maximum number of empty bands (n_{max}) are assumed to be known. Let $\mathscr{H}_0$ denote the null hypothesis or full spectrum hypothesis corresponding to the scenario where all the bands are occupied with the PU, and let $\mathscr{H}_j$ denote the jth hypothesis for which the bands in the set $L_j \neq \emptyset$ are the empty bands. The received signal $\mathbf{x}_i = [x_i(1), x_i(2), \ldots, x_i(M)]$ at the ith band is composed of M samples and can be modeled under the given hypotheses as

$$\begin{aligned} \mathscr{H}_0: \quad & \mathbf{x}_i = \mathbf{s}_i + \mathbf{v}_i && i = 1 \ldots B, \\ \mathscr{H}_j: \quad & \mathbf{x}_i = \mathbf{s}_i + \mathbf{v}_i && i \notin L_j,\ j = 1 \ldots N \\ & \mathbf{x}_i = \mathbf{v}_i && i \in L_j,\ j = 1 \ldots N \end{aligned} \tag{37}$$

If $\mathscr{H}_j$ occurs, then the task is to determine the set L_j based on the received signal $\mathbf{x}$. A given decision strategy will decompose $\mathscr{R}^{B \times M}$ into $N+1$ disjoint decision regions $(\mathscr{R}_0, \mathscr{R}_1, \ldots, \mathscr{R}_N)$ such that if $\mathbf{x} \in \mathscr{R}_j$, then the hypothesis $\mathscr{H}_j$ is assumed to be realized.

The following sections describe various methods to analyze various spectrum sensing search strategies.

5.1 Single Empty Band Detection Performance Framework

In this section, strategies for detecting and locating a single empty band in a multi-band spectrum are presented. Specifically, if the empty band is defined as j, then the

set L_j in (37) can be defined as $L_j = \{j\}, j = 1 \ldots B$. Here H_j refers to the hypothesis that j the band is empty. Hence, there are $B+1$ hypotheses, with $N = B$ $\mathscr{H}_j$ hypotheses and one full spectrum hypothesis. Based on the definition of L_j, the $\mathscr{H}_j$ and full spectrum hypotheses are defined as $\mathscr{H}_i, i = 1 \ldots B$, and $\mathscr{H}_0$, respectively with known probabilities $p(\mathscr{H}_i)$ and $p(\mathscr{H}_0)$ respectively. The strategy decides the best possible location of a single empty band.

The optimal decision strategy for the single empty band detection problem is known as the generalized likelihood ratio test (GLRT) [50]. The optimality criterion is to maximize the area under the curve (AUC) for the localized receiver operating characteristics (LROC). The probability of the false positive is

$$P_{FP} = \sum_{i=1}^{B} \int_{\mathscr{R}_i} p(\mathbf{x}|\mathscr{H}_0) d\mathbf{x} \tag{38}$$

where $\{\mathscr{R}_i\}_{i=1}^{B}$ denotes the decision regions for $\mathbf{x}$ associated with B possible empty band locations. Similarly, the probability of correctly deciding empty band, P_{TP} is defined as

$$P_{TP} = \frac{1}{1 - p(\mathscr{H}_0)} \int_{\mathscr{R}^{B\times M} - \mathscr{R}_0} \sum_{i=1}^{B} p(\mathbf{x}|\mathscr{H}_i) p(\mathscr{H}_i) d\mathbf{x} \tag{39}$$

where $R^{B\times M}$ is the complete range of $\mathbf{x}$ and $\mathscr{R}_0$ is the decision region for $\mathbf{x}$ under hypothesis $\mathscr{H}_0$. In addition, the probability of correctly locating an empty band, P_{CL}, after a true positive decision, is defined as

$$P_{CL} = \frac{1}{1 - P(\mathscr{H}_0)} \sum_{i=1}^{B} \int_{\mathscr{R}_i} p(\mathbf{x}|\mathscr{H}_i) p(\mathscr{H}_i) d\mathbf{x} \tag{40}$$

The normalization by $\frac{1}{1-P(\mathscr{H}_0)}$ in (38) and (40) are a result of each probability being conditioned to the event that there is an empty band.

The LROC is the analysis of the P_{CL} versus P_{FP} while the receiver operating characteristics (ROC) is the analysis of the P_{TP} versus P_{FP}. The optimal decision strategy

to maximize the AUC of the LROC is

$$\begin{aligned} T(\mathbf{x}) &= \min_{i\in\{1\ldots B\}} \frac{p(\mathbf{x}|\mathscr{H}_i)p(\mathscr{H}_i)}{p(\mathbf{x}|\mathscr{H}_0)} \\ i(\mathbf{x}) &= \arg\min_{i\in\{1\ldots B\}} \frac{p(\mathbf{x}|\mathscr{H}_i)p(\mathscr{H}_i)}{p(\mathbf{x}|\mathscr{H}_0)} \\ &\quad \text{Decide } \mathscr{H}_{i(x)} \text{ if } T(\mathbf{x}) < T_0, \text{ else decide } \mathscr{H}_0 \end{aligned} \tag{41}$$

5.2 Multiple Empty Bands Detection Performance Framework

In this section, decision strategies for an unknown number of empty bands are presented. The multi-band decision strategies such as the free response ROC (FROC), signal absent abscissa FROC (SAA-FROC), alternate free response ROC (AFROC), and signal absent abscissa AFROC (SAA-AFROC) are used to analyze the detection performance of multi-band spectrum sensing methods [50]. The assumption is that the prior knowledge of the input signal is not known. Hence, the spectrum sensing method used for finding an empty band is of energy detector type.

All the FROC analyses assume that the $\mathscr{H}_j$ hypothesis contain $n(n>1)$ empty bands at locations $r_1 \ldots r_n$. The goal is to find a strategy that identifies if the signal $\mathbf{x}$ contains empty-bands and if so, find the the best approximation $\hat{\mathbf{n}}$ empty bands and their approximate locations $\hat{r}_1, \ldots, \hat{r}_n$. The probability mass function (PMF) of the number of empty bands is denoted by $p_{\mathbf{n}}(n)$, and the joint PMF for the locations of these empty bands is denoted by $p_{\mathbf{r}_1\ldots\mathbf{r}_n}(r_1 \ldots r_n)$. For convenience, the number of empty bands and their locations are noted as $\theta = (n, r_1 \ldots r_n)$ and its distribution as $p_{\boldsymbol{\theta}}(\theta)$.

Estimated parameter vector is denoted as $\hat{\theta} = (\hat{n}, \hat{r}_1 \ldots \hat{r}_n)$. The likelihood ratio is

$$L(\mathbf{x}|\theta) = \frac{p(\mathbf{x}|\cup_{i=1}^{N}\mathscr{H}_i, n, r_1, \ldots, r_n)}{p(\mathbf{x}|\mathscr{H}_0)} \tag{42}$$

where $\cup_{i=1}^{N}\mathscr{H}_i$ corresponds to the union of $\mathscr{H}_j$ hypotheses.

In [50], the function $u(\theta,\hat{\theta})$ which counts the fraction of correctly located empty bands is given as

$$\begin{aligned} u(\theta,\hat{\theta}) &= \frac{\#\text{of correct localizations}}{n} \\ &= \frac{\sum_{i=1}^{n}\mathbf{1}_{\{r_i\in\{\hat{r}_1,\ldots,\hat{r}_{\hat{n}}\}\}}}{n} \end{aligned} \tag{43}$$

where $\mathbf{1}_A$ denotes the indicator function which is equal to 1 when the event A is true, and zero otherwise. The decision strategy will utilize $u(\theta,\hat{\theta})$ to weight each estimate choice, giving those choices with the most significant fraction of correctly located empty bands a high weighting factor.

AFROC is the analysis of the empty band detection fraction F_{SD} versus the probability of false positives P_{FP}. In [50], the equations to plot AFROC curve are

$$F_{SD} = \sum_{\theta} p_{\boldsymbol{\theta}}(\theta)\int_{R^{(1)}} p(\mathbf{x}|\cup_{i=1}^{N}\mathscr{H}_i,\theta)u(\theta,\hat{\theta})d\mathbf{x} \tag{44}$$

$$P_{FP} = p(\mathscr{H}_0)\int_{R^{(1)}} p(\mathbf{x}|\mathscr{H}_0)d\mathbf{x} + (1-P(\mathscr{H}_0))\sum_{\theta} p_{\boldsymbol{\theta}}(\theta)\int_{R^{(1)}} p(\mathbf{x}|\cup_{i=1}^{N}\mathscr{H}_i)v(\theta,\hat{\theta})d\mathbf{x} \tag{45}$$

where $R^{(1)} = \mathscr{R}^{B\times M} - \mathscr{R}_0$. In [50], the counting function $v(\theta,\hat{\theta})$ is defined so that it equates to one if a false localization occurs and, it equates to zero otherwise

$$v(\theta,\tilde{\theta}) = \begin{cases} 1 & N_{FL}(\theta,\tilde{\theta}) \geq 1 \\ 0 & \text{no false localizations} \end{cases}$$

where the total number of false localizations is defined as

$$N_{FL}(\theta,\tilde{\theta}) = \sum_{i=1}^{\hat{n}}\mathbf{1}_{\{\hat{r}_i\notin\{r_1,\ldots,r_n\}\}} \tag{46}$$

For the SAA-AFROC analysis, the false positives from full spectrum hypothesis bands are not counted. Hence, the second term in the definition of P_{FP} is ignored, which is same as setting $v(\theta,\hat{\theta}) = 0$.

The FROC is the analysis of the signal detection fraction F_{SD}, given in (44), versus the average number of false positives $\bar{N}_{FP}$ defined as

$$\bar{N}_{FP} = p(\mathscr{H}_0)\int_{R^{(1)}} p(\mathbf{x}|\mathscr{H}_0)\hat{n}(\mathbf{x})d\mathbf{x} + (1-P(\mathscr{H}_0))\sum_{\theta} p_{\boldsymbol{\theta}}(\theta)\int_{R^{(1)}} A(\mathbf{x},\theta,\hat{\theta})d\mathbf{x} \quad (47)$$

where $A(\mathbf{x},\theta,\hat{\theta}) = p(\mathbf{x}|\cup_{i=1}^{N}\mathscr{H}_i)N_{FL}(\theta,\hat{\theta})$, $R^{(1)} = \mathscr{R}^{B\times M} - \mathscr{R}_0$, and $N_{FL}(\theta,\hat{\theta})$ is given in (46).

Similar to SAA-AFROC curve, the decision strategy for SAA-FROC is given by removing the false positives from full spectrum hypothesis bands [50].

6 MULTI-BAND SPECTRUM SENSING ALGORITHMS

As shown in (35), the energy consumption of ADC depends on the number of samples M. The following linear, random, and binary empty band search algorithms use the fact that the ADC energy loss depends on M to calculate the energy consumption of receiver front end.

6.1 Linear Search

The goal of the linear search is to explore the spectrum from the lowest frequency to a high frequency in a sequential manner. In Fig. 21, there are B bands with signals $s_1, s_2, \ldots, s_B$ at frequencies $f_1, f_2, \ldots, f_B$. There are N empty bands and $(B-N)$ bands occupied by PUs. The bands occupied with PUs are noted as $PU_1, PU_2, \ldots, PU_{B-N}$ and the empty bands are noted by $E_1, E_2, \ldots, E_N$. As noted in Fig. 21, the linear search algorithm starts the search for empty bands from the band at frequency f_1 and then proceeds to the next band f_2. The linear search algorithm continues the search sequentially until the desired number of empty bands is found, or the search over all B bands is completed. The number of steps is the total number of bands the linear algorithm transverses. If the algorithm finds the desired number of bands in k steps, the number of samples needed for the spectrum sensing is $M \cdot k$.

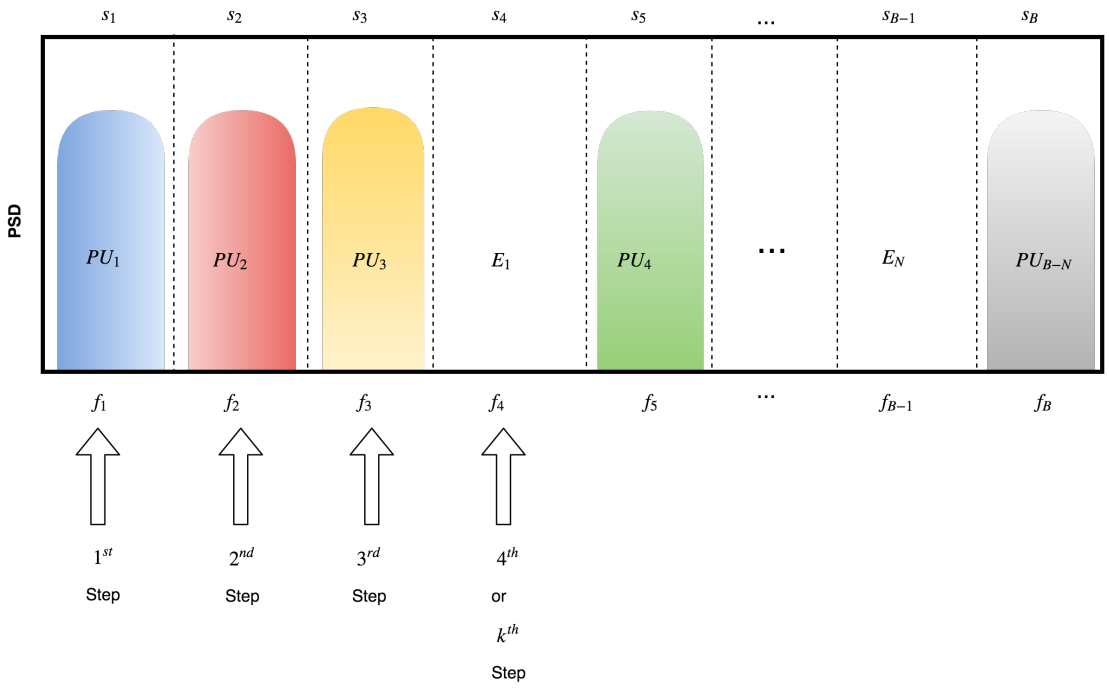

Fig. 21. Linear search.

6.2 Random Search Without Replacement

Random search without replacement looks for empty bands randomly. Unlike linear search, the frequency bands are not scanned sequentially from low to high in random search without replacement. The spectrum is scanned randomly as shown in Fig. 22. The number of steps taken by the random search without replacement is equal to the steps taken by the linear search. The random search without replacement scans a sub-band only once in one run. Similar to the linear search, if the random search without replacement algorithm finds the empty bands in k steps, the number of samples needed for the spectrum sensing is $M \cdot k$. For a constant n_{max}, k is directly proportional to B.

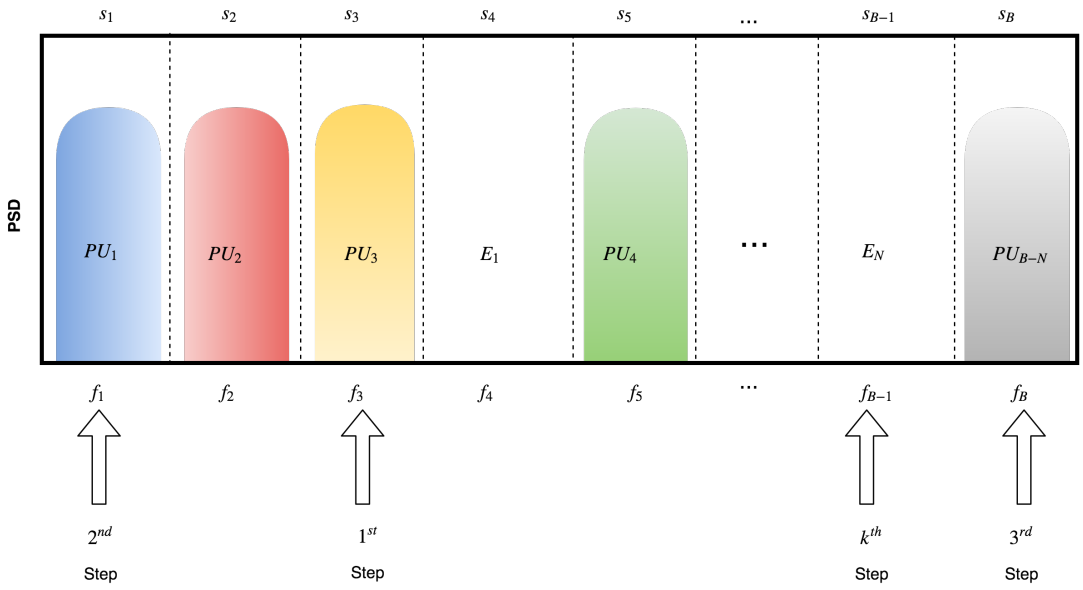

Fig. 22. Random search without replacement.

6.3 Random Search With Replacement

The random search with replacement is, as the name suggests, the pursuit of an empty band by randomly picking a sub-band out of all available bands at each trial. It is possible that the random search with replacement algorithm searches the same sub-band multiple times in one run as shown in Fig. 23. The random search with replacement algorithm usually takes more steps than the linear and the random search without replacement to find empty sub-bands.

The random search with replacement may seem unnecessary as the number of steps to find an empty band is high. However, when PUs are using the spectrum in a burst mode, the random search with replacing is handy. In a burst mode, the PU is using the spectrum for very short data transfers. The random search may look for a band occupied with a bursty PU and in the same search recheck the same band to find the band empty. Hence, the detection performance of random search with replacement may be better than the linear search.

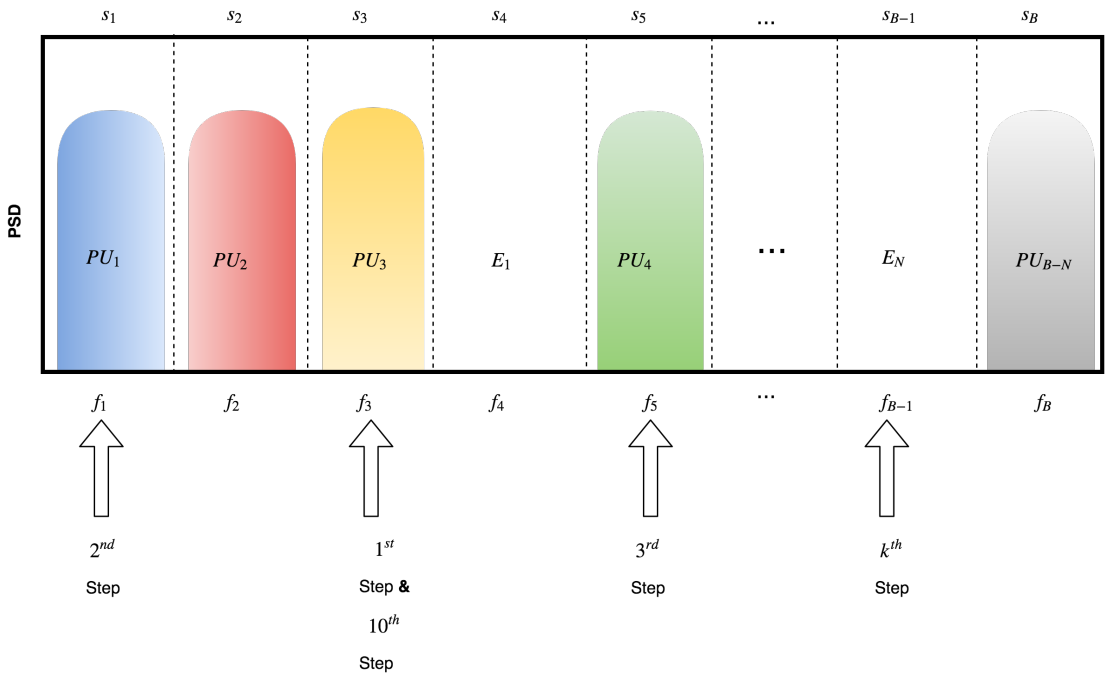

Fig. 23. Random search with replacement.

Since the energy loss of the receiver front end depends on the number of steps, the energy performance of the linear, random without replace and random with replace algorithms in terms of energy consumption can be shown as

$$E_{linear} = E_{Random w/o replace} < E_{Random w/ replace} \tag{48}$$

6.4 Binary Search

Binary search implementation is different from linear and random searches. In binary search, the spectrum is assumed to have the total number of bands as $B = 2^l$ where l is a positive integer. As shown in Fig. 24, the binary search algorithm divides the whole spectrum into two high bandwidth group of bands. For each group band, M number of samples are collected to form a test statistic. The test statistic is compared with a operating threshold to determine the possible empty group bands. If test statistics of the

left group of bands is lower than the threshold, as shown in Fig. 24, the left sub-band spectrum is further divided into two sub-bands. The same process of calculating the test statistic for threshold comparison is followed. The method of dividing and comparing continues until the algorithm finds the smallest sub-bands that are less than the threshold. The step in the binary search is the action of dividing the band as shown in Fig. 24. If at any stage, a large bandwidth sub-band group has higher energy than the threshold, each small bandwidth sub-band in the group is considered full.

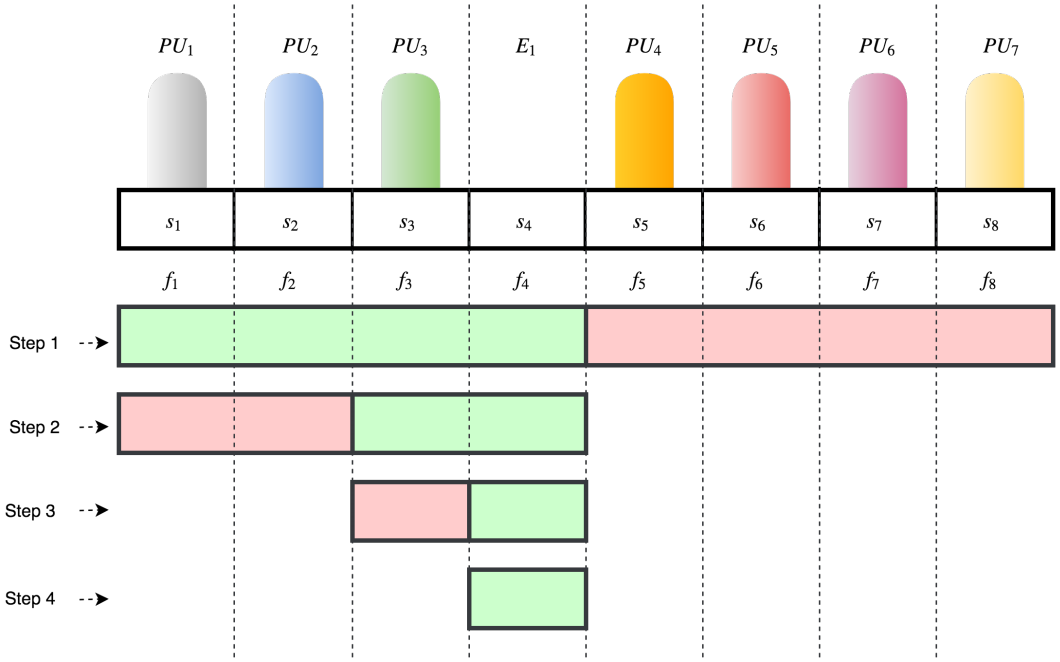

Fig. 24. Binary search.

The maximum number of steps the algorithm can take is l. The bandwidth of the group band in the first step is always higher than the bandwidth of the group band in the second step. Hence, the sampling frequency needed to sense the band reduces logarithmically as the number of steps increases. The reduction in sampling frequency results in energy saving as the energy performance of the receiver front end depends on sampling frequency as shown in (30). The noise power is proportional to the bandwidth of

the spectrum. In a narrow band, the noise power is low compared to a broader band. Hence, the detection performance of the binary search increases with the decrease in the bandwidth of the spectrum. The number of samples needed for spectrum sensing scales as $M \cdot log_2(k)$ where k is proportional to B.

Table 1
Simulation Environment

Parameters	Value
B	16
SNR	3,5,10 dB
M	10
V_{dd}	3 V
SQNR	60 dB
L_{min}	10 μm

7 SIMULATIONS AND RESULTS

Monte-Carlo simulations are used to obtain detection performance and energy curves. The effects of multipath and fading are not considered in the simulations. For simplicity, all PUs have the same SNR in the multi-band spectrum of interest. In all the simulation below, the total number of bands is B = 16. Below, we also assume $P(\mathscr{H}_0)$ = 0.5, and $P(\mathscr{H}_i) = 1/(2N)$ for $i = 1 \ldots N$, and the SU does not know about the maximum number of empty bands (n_{max}) available. In the simulations, $\hat{n}_{max}$ is the required maximum number of empty bands. The simulation is done using the Python programming language. There are no hardware measurements taken for the simulation. Values of the parameters used in the simulation are shown in Table 1.

7.1 Simulation Description

Due to the non-linearities of the RF front end circuit blocks, there is a possibility that the transmitted signal energy leaks to the surrounding bands. The leakage of energy from one band to the surrounding bands is also considered to make the simulation more applicable. In the simulation, each PU signal leaks to the surrounding two sub-bands.

A detailed description of the simulation algorithm is given in Appendix A. The PU's signal contains the samples of the transmitted data and the noise as shown in (37). Each sample of the PU's signal is modeled as the sum of two zero-mean unit variance complex Gaussian distribution samples scaled by an amplitude. The sample of the PU is scaled by

the amplitude of PU's signal and the noise sample is scaled by the noise signal amplitude. For the linear and random search methods, M samples per band are added to generate a test statistics vector to compare to a threshold. However, in the binary search method, the sub-bands have different bandwidths and contain multiple PUs. Hence, a sample of the PU is scaled as

$$S_A = \sqrt{P_x \cdot \alpha} \tag{49}$$

where S_A is the amplitude of a sample, P_x is the power of the PU's signal and α is the ratio of the total number of PUs present in the group of sub-bands to the total number of sub-bands in the group.

For example, in the step one of the binary search shown in Fig. 24, the left group of the band has three PUs in the group of four sub-bands. Hence, the value of α is $3/4$. The right group, the four red bands, in step one has the value of $\alpha = 1$ since all four bands are PUs. In binary search, the test statics is calculated using the sum of M samples generated using complex Gaussian distribution of zero-mean unit variance. Each complex Gaussian sample of PU is scaled by the amplitude determined using (49).

7.2 Single Empty-Band Detection Simulations

In single empty band detection simulation, the purpose of the SU is to find one empty band regardless of the n_{max}. As discussed in Chapter 5.1, the LROC method is used to measure the detection performance.

Based on (36), the energy consumption of the receiver front end depends on the PAPR. With an increase in the SNR, the PAPR also increases; hence, the receiver power consumption increases.

Fig. 25 shows the energy consumption for linear search, random search without replacement and random search with replacement. As expected, the energy consumption of the random search with replacement is slightly higher than the linear search and

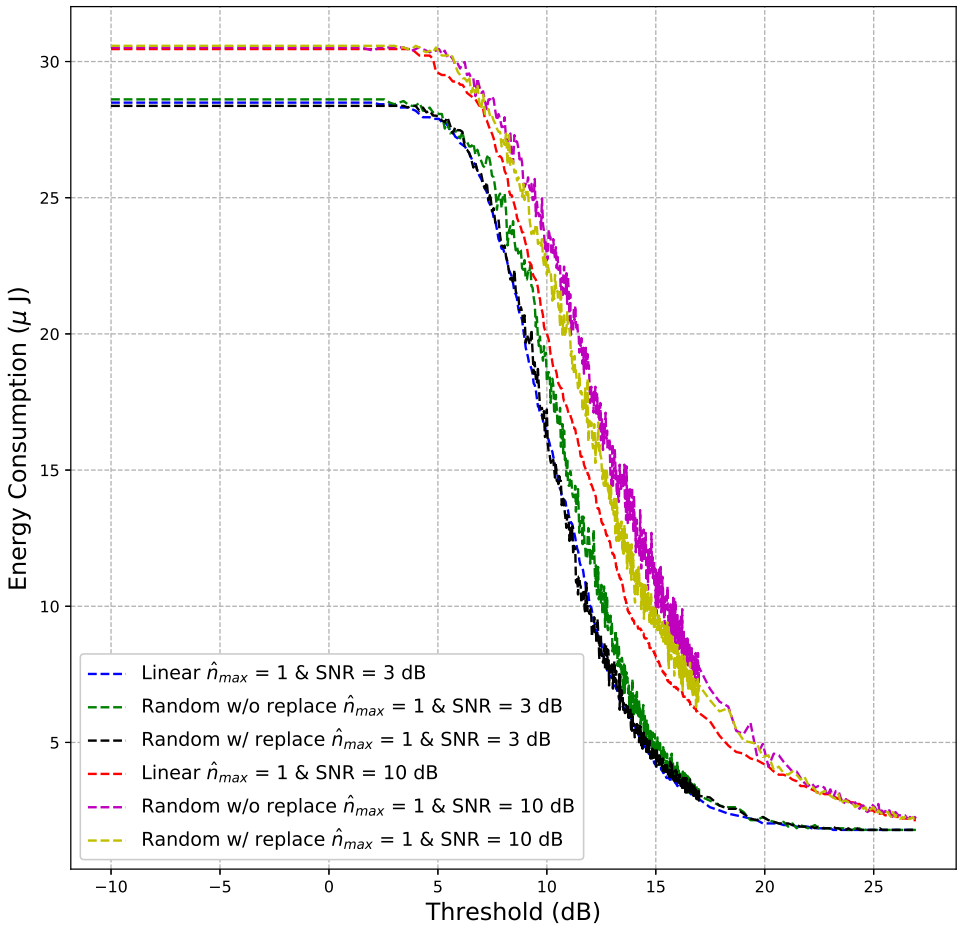

Fig. 25. Energy consumption plots for single empty band detection methods with different SNRs.

random search without replacement. Also, the energy consumption of the received signal with 3 dB SNR is lower than the signal with 10 dB SNR as expected.

Fig. 26 illustrates the energy loss of three one-band search methods with respect to the different number of empty bands. When most of the spectrum is empty and available

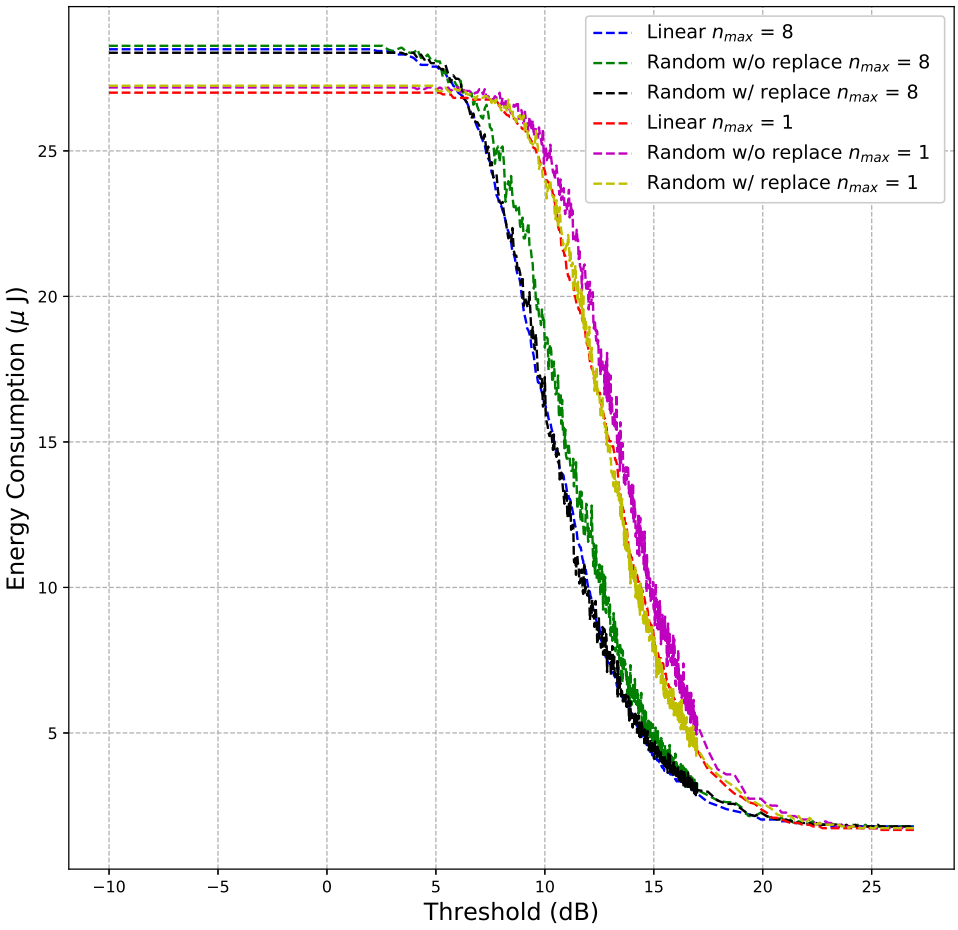

Fig. 26. Energy consumption plot for single empty band detection methods with different $\hat{n}_{max}$.

for data transfer, the number of steps taken to find the empty bands are low. The energy consumption of the scenario where more empty bands are available should be lower compared to the situation where less empty bands are available. As expected, the energy

consumption is lower when there are eight empty bands available compared to four empty band scenario.

7.3 Multiple Empty-Band Detection Simulations

In multi-band spectrum sensing, the goal of the algorithms is to find more than one empty band efficiently. The linear search, random search, and binary search are the three most straightforward algorithms to locate multiple empty bands in a multi-band spectrum. In this section, simulations of multi-band spectrum sensing algorithms using the framework of energy consumption and detection performance are presented.

Fig. 27, 28 show the FROC analysis of the linear search algorithm with respect to the thresholds for $\hat{n}_{max} = 2$ and $\hat{n}_{max} = 4$. The SNR of the simulation is set to 10 dB for $n_{max} = 4$. Fig. 28 also shows the energy loss of the ADC as a function of the thresholds. The energy loss of the ADC is normalized by 28.2 μJ. In Fig. 28, the number of the average false positive fraction is greater than one as anticipated. Therefore, the average number of false positive is plotted separately. The energy loss of the ADC decreases with an increase in the false positive rate. As the AUC of true positive rate plot increases, the AUC of the energy plot decreases. Low AUC for the energy plot means good energy efficiency.

Fig. 27, 29 show the SAA-FROC investigation with respect to the thresholds in the simulation environment where SNR is 3 dB and $n_{max} = 4$. The linear search algorithm is used to detect two and four empty bands in the spectrum. Average false positive plots in Fig. 29 show the detection performance analysis respect to the thresholds.

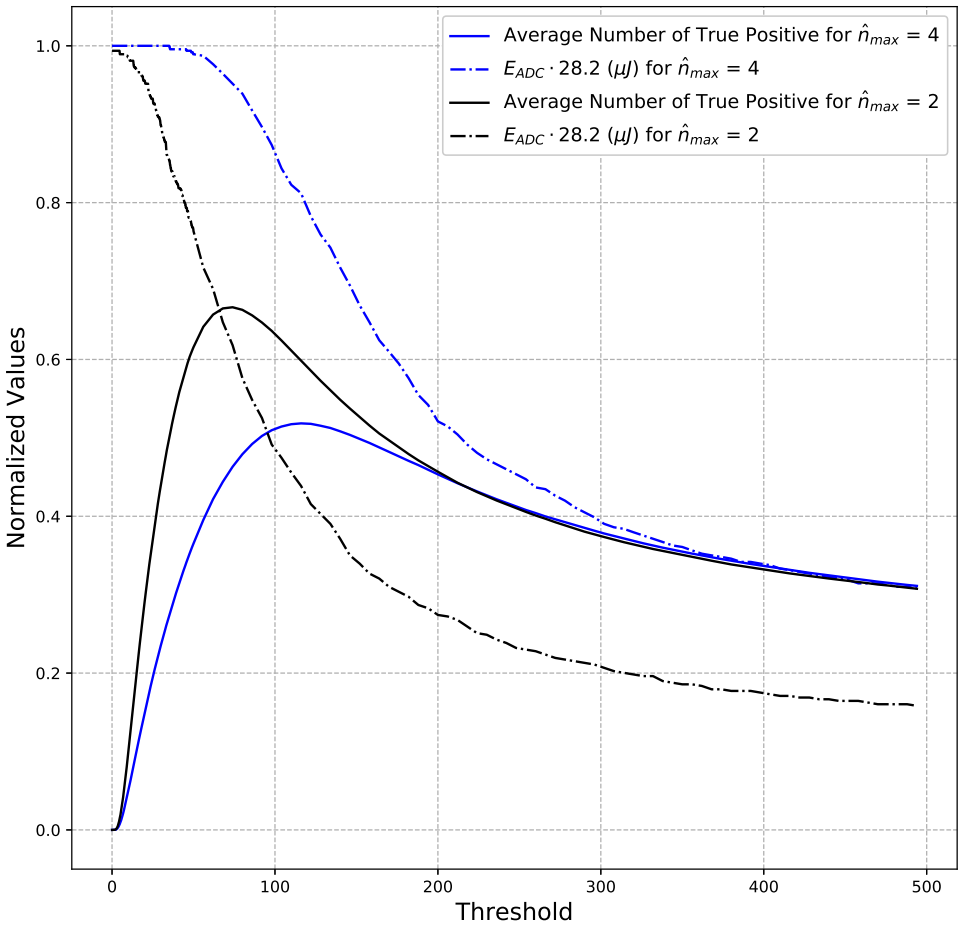

Fig. 27. Energy consumption and true detection performance analysis of the linear search spectrum sensing method using the FROC and SAA-FROC frameworks.

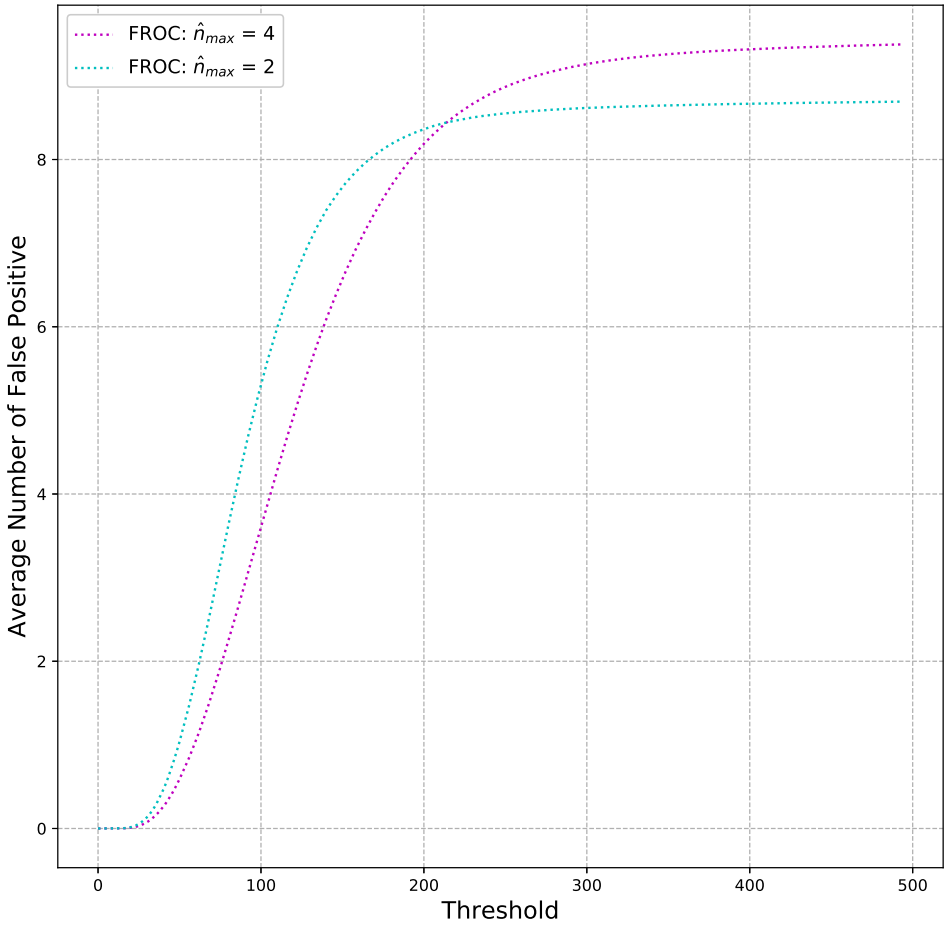

Fig. 28. False detection performance analysis of the linear search spectrum sensing method using the FROC framework.

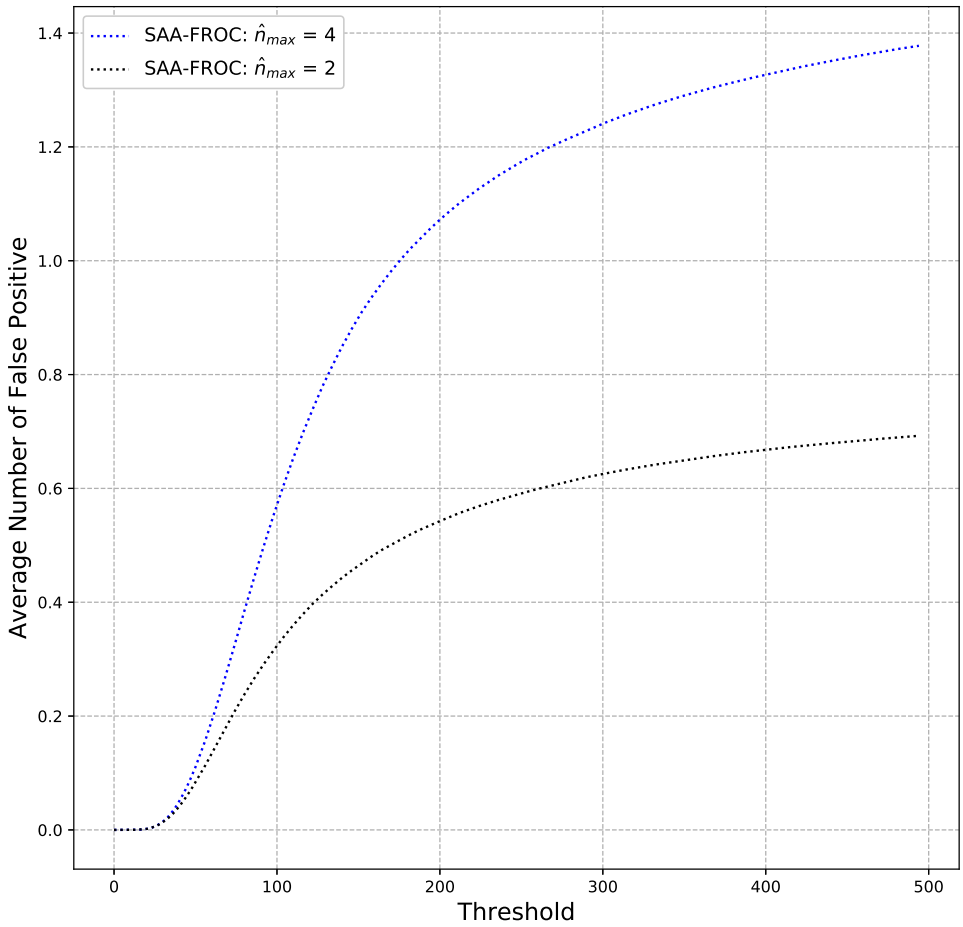

Fig. 29. False detection performance analysis of the linear search spectrum sensing method using the SAA-FROC framework.

Fig. 30 displays the AFROC performance framework along with the energy dissipation of the ADC for the thresholds. The simulation is done with n_{max} = 1 and SNR of 5 dB. The AUC for the true positive fraction is very low because the algorithm searches for two and four empty bands where there is only one empty band available.

Since most of the spectrum is full with PU's activity, the algorithm takes more steps to find empty bands. The false positive fraction reaches to one quickly. At the peak of the true positive rate curve, both the energy dissipation of the ADC and the false positive rate are high. Hence, the detection performance is poor.

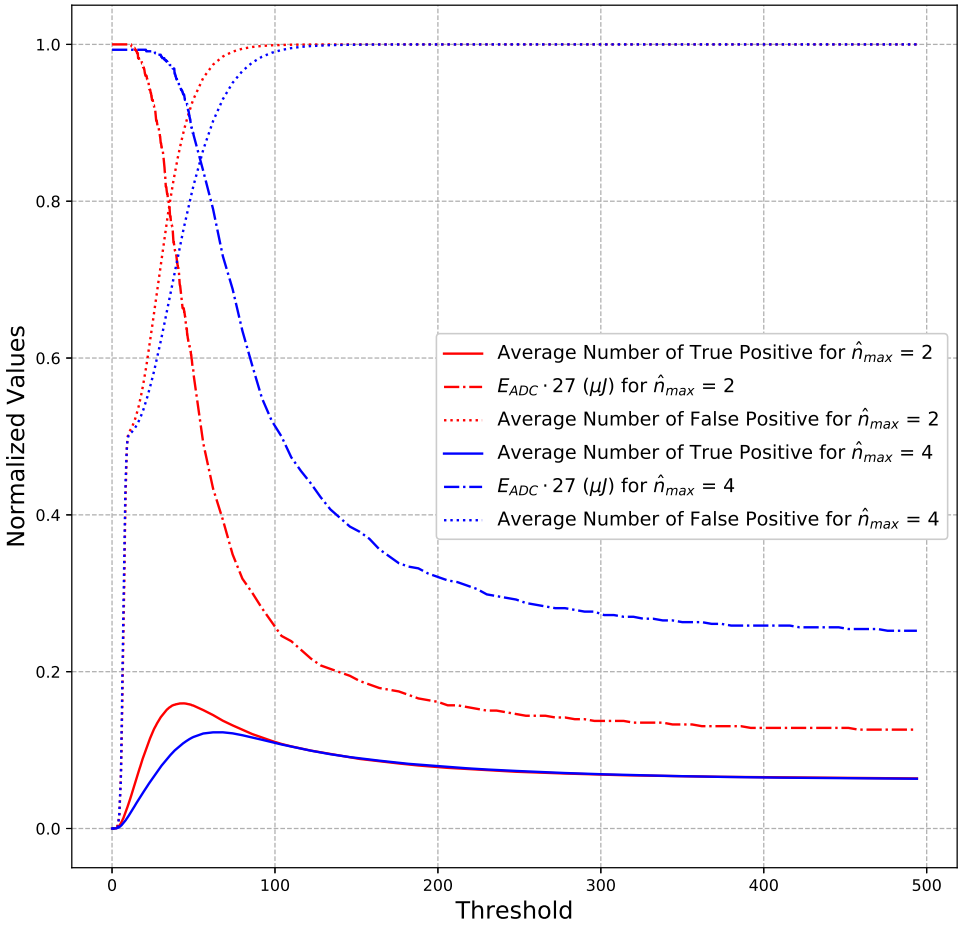

Fig. 30. Energy consumption and detection performance analysis of the linear search spectrum sensing method using the AFROC framework.

Fig. 31 exhibit the interpretation of the SAA-AFROC framework in conjunction with the energy consumption of the ADC. The simulation environment includes SNR of 3 dB and n_{max} = 8. The plot of the false positive fraction, the true positive fraction, and the energy loss of the ADC is shown to examine the behavior of the receiver front end energy loss with respect to the detection performance of the spectrum sensing algorithm.

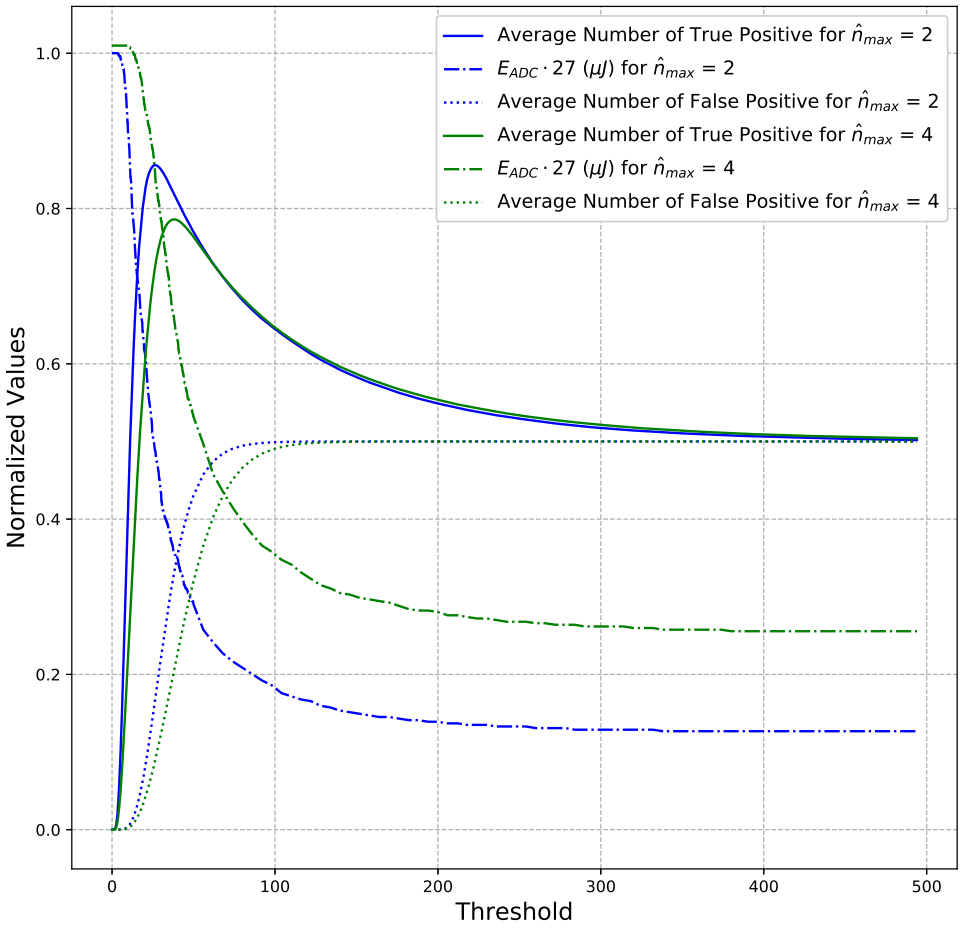

Fig. 31. Energy consumption and detection performance analysis of the linear search spectrum sensing method using the SAA-AFROC framework.

Fig. 32 shows the FROC performance plot of the linear and binary search. The plot was simulated with the SNR of 3 dB and n_{max} = 4. The AUC for the linear search is higher than the binary search. Therefore, the linear search performs better than the binary search. However, Fig. 33 shows that the binary search has the lowest energy consumption.

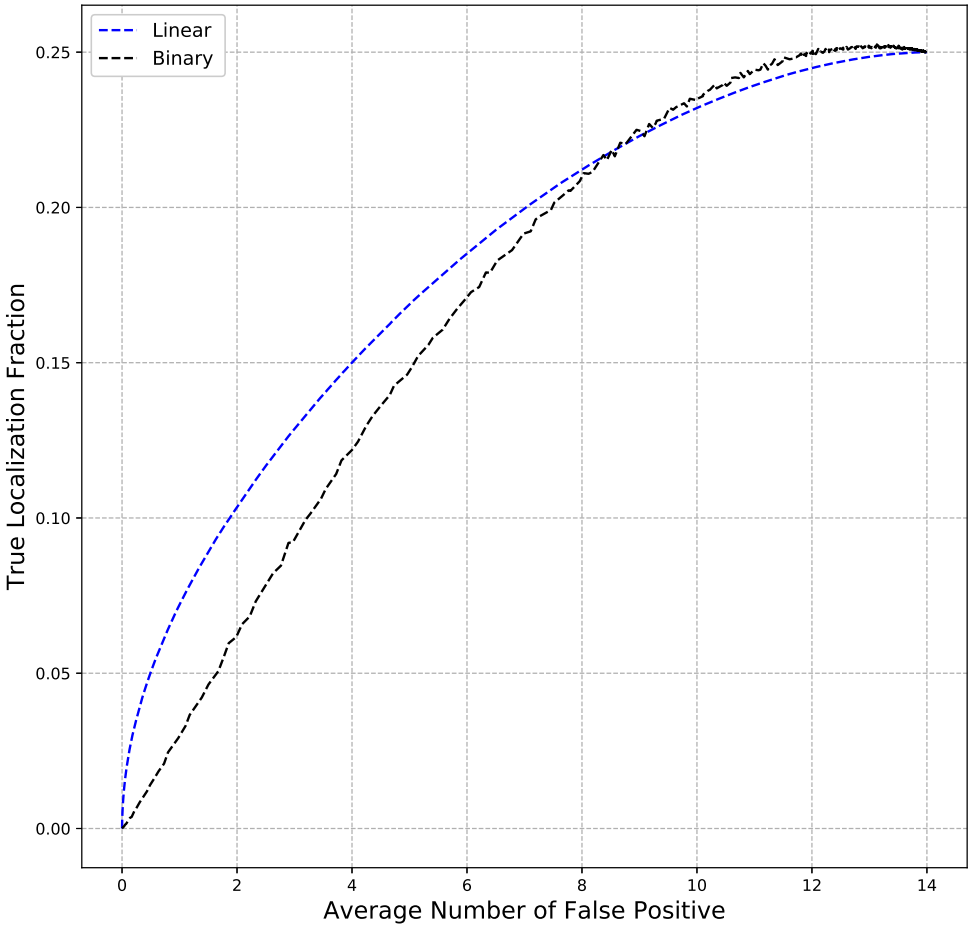

Fig. 32. FROC analysis plot for the linear and binary search methods.

Hence, the binary search is energy efficient but delivers lower detection performance than the linear search.

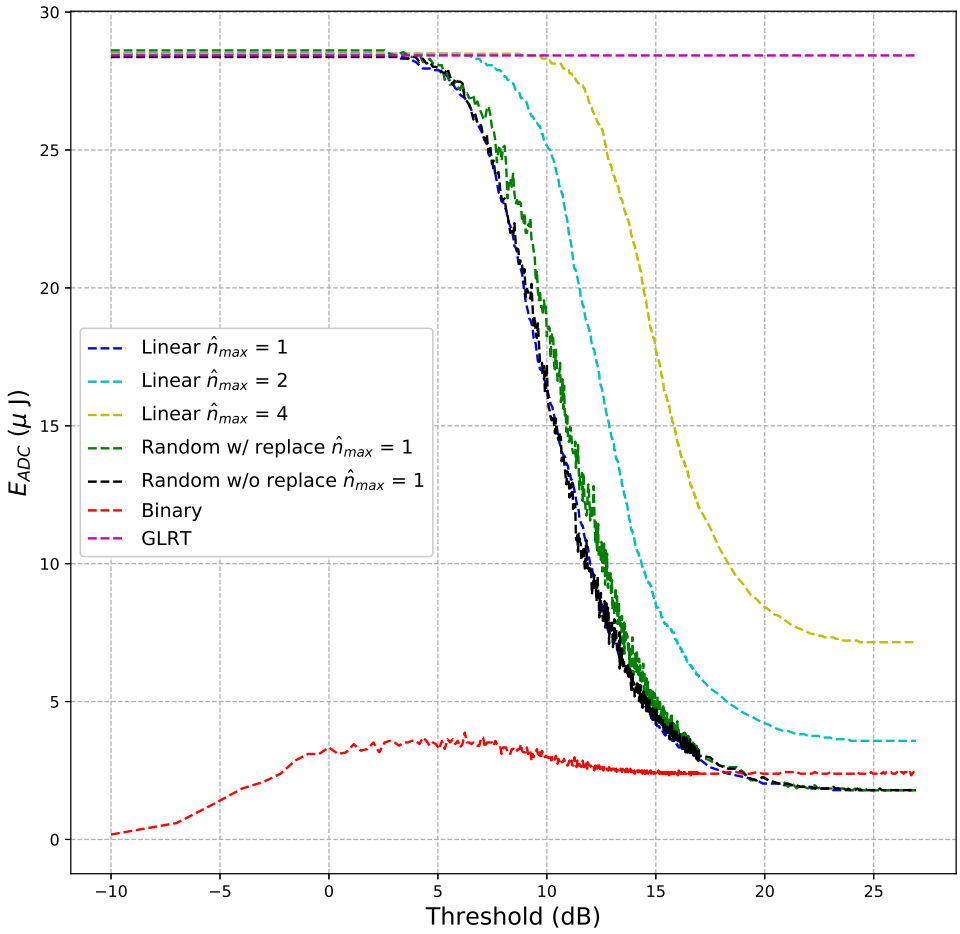

Fig. 33. Energy consumption plots for multiple empty band detection methods with respect to the threshold.

Fig. 33 shows the energy consumption plots for the GLRT, binary search, linear search, random search without replacement, and random search with replacement. The

linear search with $\hat{n}_{max} = 1$, random search without replacement, and random search with replacement strategies only find one empty band while the GLRT and binary search find multiple empty bands. The GLRT search method requires the knowledge of all the sub-bands available in the multi-band spectrum. Hence, the energy performance of the GLRT search does not depend on the number of steps. The energy consumption is the highest for GLRT and does not rely on the threshold. The linear search and random search without replacement strategies have similar energy consumption curves for $\hat{n}_{max} = 1$. The energy loss of the random search with replacement is marginally higher than the linear search for $\hat{n}_{max} = 1$. The linear search, random search without replacement, and random search with replacement strategies have high energy consumption at low thresholds as the algorithm searches the majority of the spectrum bands. As the threshold increases, energy consumption decreases. The binary search has the lowest energy consumption. As $\hat{n}_{max}$ increase to 2, the energy consumption of the linear search is higher for the same threshold compared to linear search with $\hat{n}_{max} = 1$. Similarly, the energy loss is high for linear search with $\hat{n}_{max} = 4$ compared to the linear search with $\hat{n}_{max} = 2$ as expected.

8 CONCLUSIONS AND FUTURE WORK

In this paper, a framework to analyze multi-band spectrum search techniques in terms of energy and detection performance is introduced. The ability to have the information on the energy consumption of the receiver front end for a particular spectrum sensing algorithm is the most significant advantage of the proposed framework. Most of the previous analyses only focused on the empty-band detection performance of the multi-band spectrum sensing algorithm. The framework proposed in this research not only elaborates the performance analysis of correctly identifying one or multiple empty bands but also provides information on the energy loss of the receiver.

The scope of the future work of the research presented in this paper is large. The critical assumption in the study is that PUs operate on the same the SNR. However, the SNR of each PU in the multi-band spectrum environment is not the same in practical situations. Hence, a modified framework to estimate the SNR of the PU can be developed based on the presented work. The threshold is also considered constant for all of the bands in the energy detection method. The technique of adaptive threshold can be incorporated into the presented study to make the framework even more generalized.

The model manifested in this study to analyze the multi-band spectrum sensing algorithms does not include phenomena like multi-path and fading. Multi-path and fading are inevitable in communications systems. Hence, incorporating the concepts of multiple wireless channels can make the model robust and versatile. The presented research is based on the energy detection method. Hence, the spectrum of wideband code-division multiple access modulation cannot be detected through the model presented in this investigation. The techniques of machine learning can be used to detect wideband signals that are below the noise spectrum.

Literature Cited

[1] P. V. Paul and R. Saraswathi, "The internet of things — a comprehensive survey," in *2017 International Conference on Computation of Power, Energy Information and Commuincation (ICCPEIC)*, pp. 421–426, March 2017.

[2] A. A. Khan, M. H. Rehmani, and A. Rachedi, "Cognitive-radio-based internet of things: Applications, architectures, spectrum related functionalities, and future research directions," *IEEE Wireless Communications*, vol. 24, pp. 17–25, June 2017.

[3] G. Hattab and M. Ibnkahla, "Multiband spectrum access: Great promises for future cognitive radio networks," *Proceedings of the IEEE*, vol. 102, 02 2014.

[4] A. Ali and W. Hamouda, "Advances on spectrum sensing for cognitive radio networks: Theory and applications," *IEEE Communications Surveys Tutorials*, vol. 19, pp. 1277–1304, Secondquarter 2017.

[5] A. Ahmad, S. Ahmad, M. H. Rehmani, and N. U. Hassan, "A survey on radio resource allocation in cognitive radio sensor networks," *IEEE Communications Surveys Tutorials*, vol. 17, pp. 888–917, Secondquarter 2015.

[6] B. Wang and K. J. R. Liu, "Advances in cognitive radio networks: A survey," *IEEE Journal of Selected Topics in Signal Processing*, vol. 5, pp. 5–23, Feb 2011.

[7] J. M. Khurpade, D. Rao, and P. D. Sanghavi, "A survey on iot and 5g network," in *2018 International Conference on Smart City and Emerging Technology (ICSCET)*, pp. 1–3, Jan 2018.

[8] Y. Li, B. Bakkaloglu, and C. Chakrabarti, "A system level energy model and energy-quality evaluation for integrated transceiver front-ends," *IEEE Transactions on Very Large Scale Integration (VLSI) Systems*, vol. 15, pp. 90–103, Jan 2007.

[9] V. Gianni, J. Craninckx, and A.Basxhirotto, *Baseband Analog Circuits for Software Defined Radio*. Dordrecht, The Netherlands: Springer, 2008.

[10] S. Hori, T. Maeda, N. Matsuno, and H. Hida, "Low-power widely tunable gm-c filter with an adaptive dc-blocking, triode-biased mosfet transconductor," in *Proceedings of the 30th European Solid-State Circuits Conference*, pp. 99–102, Sep. 2004.

[11] H. Gao, Y. Wu, M. Matters-Kammerer, D. Milosevic, J. M. G. Linnartz, and P. Baltus, "System analysis and energy model of 60ghz radio-triggered wireless sensor receiver," in *2013 IEEE 20th Symposium on Communications and Vehicular Technology in the Benelux (SCVT)*, pp. 1–4, Nov 2013.

[12] L. Lolis, M. de Souza, L. B. Zambon, and A. Mariano, "Impact of a fully reconfigurable lna on an rf front-end: A system level analysis," in *2014 21st IEEE International Conference on Electronics, Circuits and Systems (ICECS)*, pp. 662–665, Dec 2014.

[13] T.-Y. Chiou, D. Gebre-Egziabher, T. Walter, and P. Enge, "Model analysis on the performance for an inertial aided fll-assisted-pll carrier-tracking loop in the presence of ionospheric scintillation," in *Proceedings of the ION National Technical Meeting*, pp. 1276–1295, 2007.

[14] B. Murmann, "Adc performance survey 1997–2015," 2015.

[15] P. Heydari, "Design considerations for low-power ultra wideband receivers," in *Sixth international symposium on quality electronic design (isqed'05)*, pp. 668–673, March 2005.

[16] A. Ranjan, , and B. Singh, "Design and analysis of spectrum sensing in cognitive radio based on energy detection," in *2016 International Conference on Signal and Information Processing (IConSIP)*, pp. 1–5, Oct 2016.

[17] J. Zhu, Z. Xu, F. Wang, B. Huang, and B. Zhang, "Double threshold energy detection of cooperative spectrum sensing in cognitive radio," in *2008 3rd International Conference on Cognitive Radio Oriented Wireless Networks and Communications (CrownCom 2008)*, pp. 1–5, May 2008.

[18] A. Muralidharan, P. Venkateswaran, S. G. Ajay, D. Arun Prakash, M. Arora, and S. Kirthiga, "An adaptive threshold method for energy based spectrum sensing in cognitive radio networks," in *2015 International Conference on Control, Instrumentation, Communication and Computational Technologies (ICCICCT)*, pp. 8–11, Dec 2015.

[19] P. Semba Yawada and A. J. Wei, "Cyclostationary detection based on non-cooperative spectrum sensing in cognitive radio network," in *2016 IEEE International Conference on Cyber Technology in Automation, Control, and Intelligent Systems (CYBER)*, pp. 184–187, June 2016.

[20] H. N. Abdullah and H. S. Abed, "Improvement of energy consumption in cognitive radio by reducing the number of sensed samples," in *2016 Al-Sadeq International Conference on Multidisciplinary in IT and Communication Science and Applications (AIC-MITCSA)*, pp. 1–6, May 2016.

[21] G. Vijay, E. B. A. Bdira, and M. Ibnkahla, "Cognition in wireless sensor networks: A perspective," *IEEE Sensors Journal*, vol. 11, pp. 582–592, March 2011.

[22] M. Damavandi and S. Nader-Esfahani, "Compressive wideband spectrum sensing in cognitive radio systems based on cyclostationary feature detection," in *2015 9th International Conference on Next Generation Mobile Applications, Services and Technologies*, pp. 282–287, Sep. 2015.

[23] C. Jiang, Y. Li, W. Bai, Y. Yang, and J. Hu, "Statistical matched filter based robust spectrum sensing in noise uncertainty environment," in *2012 IEEE 14th International Conference on Communication Technology*, pp. 1209–1213, Nov 2012.

[24] Q. Lv and F. Gao, "Matched filter based spectrum sensing and power level recognition with multiple antennas," in *2015 IEEE China Summit and International Conference on Signal and Information Processing (ChinaSIP)*, pp. 305–309, July 2015.

[25] S. A. Jain and M. M. Deshmukh, "Performance analysis of energy and eigenvalue based detection for spectrum sensing in cognitive radio network," in *2015 International Conference on Pervasive Computing (ICPC)*, pp. 1–5, Jan 2015.

[26] B. Zayen, A. Hayar, and K. Kansanen, "Blind spectrum sensing for cognitive radio based on signal space dimension estimation," in *2009 IEEE International Conference on Communications*, pp. 1–5, June 2009.

[27] B. Khalfi, A. Zaid, and B. Hamdaoui, "When machine learning meets compressive sampling for wideband spectrum sensing," in *2017 13th International Wireless Communications and Mobile Computing Conference (IWCMC)*, pp. 1120–1125, June 2017.

[28] A. M. Mikaeil, B. Guo, and Z. Wang, "Machine learning to data fusion approach for cooperative spectrum sensing," in *2014 International Conference on Cyber-Enabled Distributed Computing and Knowledge Discovery*, pp. 429–434, Oct 2014.

[29] G. Hattab and M. Ibnkahla, "Multiband spectrum access: Great promises for future cognitive radio networks," *Proceedings of the IEEE*, vol. 102, pp. 282–306, March 2014.

[30] H. Joshi, H. H. Sigmarsson, S. Moon, D. Peroulis, and W. J. Chappell, "High-q fully reconfigurable tunable bandpass filters," *IEEE Transactions on Microwave Theory and Techniques*, vol. 57, pp. 3525–3533, Dec 2009.

[31] X. Han, W. Xu, K. Niu, and Z. He, "A novel wavelet-based energy detection for compressive spectrum sensing," in *2013 IEEE 77th Vehicular Technology Conference (VTC Spring)*, pp. 1–5, June 2013.

[32] Z. Tian and G. B. Giannakis, "A wavelet approach to wideband spectrum sensing for cognitive radios," in *2006 1st International Conference on Cognitive Radio Oriented Wireless Networks and Communications*, pp. 1–5, June 2006.

[33] L. Xu and M. Xue, "Selection of optimal wavelet basis for singularity detection of non-stationary signal," in *2011 International Conference on Electrical and Control Engineering*, pp. 4959–4962, Sep. 2011.

[34] Z. Quan, S. Cui, A. H. Sayed, and H. V. Poor, "Optimal multiband joint detection for spectrum sensing in cognitive radio networks," *IEEE Transactions on Signal Processing*, vol. 57, pp. 1128–1140, March 2009.

[35] S. Z. Farooq and A. Ghafoor, "Multiband sensing-time-adaptive joint detection cognitive radios framework for gaussian channels," in *Proceedings of 2013 10th International Bhurban Conference on Applied Sciences Technology (IBCAST)*, pp. 406–411, Jan 2013.

[36] B. Farhang-Boroujeny, "Filter bank spectrum sensing for cognitive radios," *IEEE Transactions on Signal Processing*, vol. 56, pp. 1801–1811, May 2008.

[37] I. Raghu, S. S. Chowdary, and E. Elias, "Efficient spectrum sensing for cognitive radio using cosine modulated filter banks," in *2016 IEEE Region 10 Conference (TENCON)*, pp. 2086–2089, Nov 2016.

[38] D. L. Donoho, "Compressed sensing," *IEEE Transactions on Information Theory*, vol. 52, pp. 1289–1306, April 2006.

[39] E. J. Candes and M. B. Wakin, "An introduction to compressive sampling," *IEEE Signal Processing Magazine*, vol. 25, pp. 21–30, March 2008.

[40] A. Mahram, M. G. Shayesteh, and S. B. Kordan, "A novel wideband spectrum sensing algorithm for cognitive radio networks based on doa estimation model," in *6th International Symposium on Telecommunications (IST)*, pp. 359–362, Nov 2012.

[41] T. Luan, L. Dong, K. Xiao, and X. Zhang, "Blind multiband joint detection in cognitive radio networks based on model selection," in *2010 6th International Conference on Wireless Communications Networking and Mobile Computing (WiCOM)*, pp. 1–4, Sep. 2010.

[42] G. N. Nazarova, V. V. Elesin, G. V. Chukov, D. M. Amburkin, and A. Y. Nikiforov, "Long-term transient radiation effects in soi cmos rf ics," in *2015 15th European Conference on Radiation and Its Effects on Components and Systems (RADECS)*, pp. 1–4, Sep. 2015.

[43] P. Chopra, N. Kumar, and R. Paily, "Ultra wideband agc and vga designs for software radio applications," in *TENCON 2008 - 2008 IEEE Region 10 Conference*, pp. 1–5, Nov 2008.

[44] A. Motamed, , and M. Ismail, "A low-voltage low-power wide-range cmos variable gain amplifier," *IEEE Transactions on Circuits and Systems II: Analog and Digital Signal Processing*, vol. 45, pp. 800–811, July 1998.

[45] M. Laddomada, F. Daneshgaran, M. Mondin, and R. M. Hickling, "A pc-based software receiver using a novel front-end technology," *IEEE Communications Magazine*, vol. 39, pp. 136–145, Aug 2001.

[46] T. Song, H. Oh, E. Yoon, and S. Hong, "A low-power 2.4-ghz current-reused receiver front-end and frequency source for wireless sensor network," *IEEE Journal of Solid-State Circuits*, vol. 42, pp. 1012–1022, May 2007.

[47] E. Lauwers and G. Gielen, "Power estimation methods for analog circuits for architectural exploration of integrated systems," *IEEE Transactions on Very Large Scale Integration (VLSI) Systems*, vol. 10, pp. 155–162, April 2002.

[48] S. Cui, A. J. Goldsmith, and A. Bahai, "Energy-constrained modulation optimization," *IEEE Transactions on Wireless Communications*, vol. 4, pp. 2349–2360, Sep. 2005.

[49] S. Cui, A. J. Goldsmith, and A. Bahai, "Energy-efficiency of mimo and cooperative mimo techniques in sensor networks," *IEEE Journal on Selected Areas in Communications*, vol. 22, pp. 1089–1098, Aug 2004.

[50] S. D. Collins and B. Sirkeci-Mergen, "Localization roc analysis for multiband spectrum sensing in cognitive radios," in *MILCOM 2013 - 2013 IEEE Military Communications Conference*, pp. 64–67, Nov 2013.

Appendix A

SIMULATION ALGORITHM

The simulation for linear and random search is done using Algorithm 1. Algorithm 1 begins with the initialization of the required variables. Within one trial of the simulation, the spectrum containing B sub-bands is constructed using randomly picked PU's locations. At each sub-band, M samples of noise or a PU's signal power plus noise is added. The leakage of the signal energy to the surrounding bands is also calculated. After preparing an energy vector using the received samples, linear and random search methods are used to find empty bands. The energy loss is measured using (35). The detection performance evaluating parameters such as true localization, true detection, false localization, and false detection are determined based on the search method results. Table 2 contains the references to the notation used in Algorithm 1.

Table 2
Simulation Notation

Symbol	Meaning
B	Total number of bands.
M	Number of samples to be collected per band.
L_{SNR}	The set of the SNR values.
D_t	The set of thresholds.
σ_i^2	The variance of signal i.
E_{ADC}	The set of calculated ADC energy.
N_I	The size of set I.
T_1	The total number of trials.
T_2	Trials per threshold.
X	The received signal.
E_X	Energy vector of the received signal.
s, v	The PU and noise signal respectively.
$G \sim (m, \sigma^2)$	Gaussian distribution with mean of m and variance of σ^2.
$U \sim (a, b)$	Uniform distribution in the range from a to b.
P	The set containing locations of PUs.
E_l	The leakage energy vector.
$\lvert \cdot \rvert^2$	The square of the absolute value.
S	The vector of number of steps.
$Search(E, \text{Th})$	A spectrum search method that finds bands b that are less than the the threshold Th.
$Energy(E, smp)$	The method that calculates the energy of a vector E based on the number of samples (smp).

Algorithm 1 The Simulation Algorithm for Linear and Random Search

// Initialize variables
$B \leftarrow 16$
$M \leftarrow 10$
$L_{\text{SNR}} \leftarrow 3, 5, 10$
$D_t \leftarrow (0 : 0.1 : 500)$
for $kk \in L_{\text{SNR}}$ **do**
    $\sigma_s^2 \leftarrow L_{\text{SNR}}[kk]$
    $E_{\text{ADC}}(0 : N_{T_1}, 0 : N_{D_t}) \leftarrow 0$
    $T_l(0 : N_{T_1}, 0 : N_{D_t}) \leftarrow 0$
    $T_r(0 : N_{T_1}, 0 : N_{D_t}) \leftarrow 0$
    $\text{SNR} \leftarrow \frac{\sigma_s^2}{\sigma_v^2}$
    for $jj \in T_1$ **do**
        for $ii \in T_2$ **do**
            $X(0 : N_B) \leftarrow 0$
            $E_X(0 : N_B) \leftarrow 0$
            $P(0 : k) \leftarrow U \sim (0, B)$
            for $i \in B$ **do**
                if $i \in P$ **then** ▷ PU signal
                    for $j \in M$ **do**
                        $s \leftarrow G \sim (0, \sigma_s^2)$
                        $v \leftarrow G \sim (0, \sigma_v^2)$
                        $X(i) \leftarrow s + v$
                        $E_X(i) \leftarrow E_X(i) + |X(i)|^2$
                        $E_X \leftarrow E_l$ ▷ Adding spectrum leakage
                if $i \notin P$ **then** ▷ Noise only signal
                    for $j \in M$ **do**
                        $v \leftarrow G \sim (0, \sigma_v^2)$
                        $X(i) \leftarrow v$
                        $E_X(i) \leftarrow E_X(i) + |X(i)|^2$
            $S(0 : N_{D_t}) \leftarrow 0$
            for $i \in D_t$ **do**
                $b, S(i) \leftarrow Search(E_X, Dt(i))$ ▷ Various search methods
                $E_{\text{ADC}}(jj, i) \leftarrow Energy(E_X, M \cdot S(i))$
                if $b \neq -1$ **then** ▷ True localization determination
                    $T_r(jj, i) \leftarrow T_r(jj, i) + 1$
                    if $b \in P$ **then**
                        $T_l(jj, i) \leftarrow T_l(jj, i) + 1$